Palaeogeography, Palaeoclimatology, Palaeoecology 560 (2020) 110027

Contents lists available at ScienceDirect

Palaeogeography, Palaeoclimatology, Palaeoecology

journal homepage: www.elsevier.com/locate/palaeo

Climate variability during MIS 20–18 as recorded by alkenone-SST and calcareous plankton in the Ionian Basin (central Mediterranean)

Maria Marino[a,*], Angela Girone[a], Salvatore Gallicchio[a], Timothy Herbert[b], Marina Addante[a], Pietro Bazzicalupo[a], Ornella Quivelli[a], Franck Bassinot[c], Adele Bertini[d], Sebastien Nomade[c], Neri Ciaranfi[a], Patrizia Maiorano[a]

[a] Dipartimento di Scienze della Terra e Geoambientali, University of Bari, Italy
[b] Brown University, Providence, RI, USA
[c] Laboratoire des Sciences du Climat et de L'Environnement, UMR8212, LSCE/IPSL, CEA-CNRS-UVSQ and Université Paris-Saclay, Gif-Sur-Yvette, France
[d] Dipartimento di Scienze della Terra, University of Florence, Italy

ARTICLE INFO

Keywords:
Lower-Middle Pleistocene
MIS 19
Southern Italy
Marine biomarkers
Coccolithophores
Planktonic foraminifera

ABSTRACT

This study shows the first Mediterranean high-resolution record of alkenone-derived sea surface temperature (SST) in the marine sediments outcropping at the Ideale section (IS) (southern Italy, central Mediterranean) from late marine isotope stage (MIS) 20 - through early MIS 18. The SST pattern evidences glacial-interglacial up to submillennial-scale temperature variation, with lower values (~13 °C) in late MIS 20 and substage 19b, and higher values (up to 21 °C) in MIS 19c and in the interstadials of MIS 19a. The SST data are combined with the new calcareous plankton analysis and the available, chronologically well-constrained carbon and oxygen isotope records in the IS. The multi-proxy approach, together with the location of the IS near the Italian coasts, the lower circalittoral-upper bathyal depositional setting, and high sedimentation rate allow to document long-and short-term paleoenvironmental modifications (sea level, rainfall, inorganic/organic/fresh water input to the basin), as a response to regional and global climate changes. The combined proxies reveal the occurrence of a terminal stadial event in late MIS 20 (here Med-H_{TIX}), and warm-cold episodes (here Med-BA_{TIX} and Med-YD_{TIX}) during Termination IX (TIX), which recall those that occurred through the last termination (TI). During these periods and the following ghost sapropel layer (insolation cycle 74, 784 ka) in the early MIS 19, high frequency internal changes are synchronously recorded by all proxies. The substage MIS 19c is warm but quite unstable, with several episodes of paleoenvironmental changes, associated with fluctuating tropical-subtropical water inflow through the Gibraltar Strait, variations of the cyclonic regime in the Ionian basin, and the southward shift of westerly winds and winter precipitation over southern Europe and Mediterranean basin. Three high-amplitude millennial-scale oscillations in the patterns of SST and calcareous plankton key taxa during MIS 19a are interpreted as linked to changes in temperature as well as in salinity due to periodical water column stratification and mixing.

The main processes involved in the climate variability include changes in oceanographic exchanges through the Gibraltar Strait during modulations of Atlantic meridional overturning circulation and/or variations in atmospheric dynamics related to the influence of westerly and polar winds acting in the paleo-Ionian basin. A strong climate teleconnection between the North Atlantic and Mediterranean is discussed, and a prominent role of atmospheric processes in the central Mediterranean is evidenced by comparing data sets at the IS with Italian and extra-Mediterranean marine and terrestrial records.

1. Introduction

Marine Isotope Stage (MIS) 19 is generally considered an excellent analogue for the current interglacial, due to the same astronomical configuration of orbital parameters: low eccentricity and an obliquity maximum almost in phase with the northern Hemisphere precession minimum. For this reason, any high-resolution study of MIS 19 can bring invaluable pieces of information about the natural duration of the current interglacial and the inception of next glacial in absence of human impact. MIS 19 is characterized by an orbital/suborbital climate

* Corresponding author.
E-mail address: maria.marino@uniba.it (M. Marino).

https://doi.org/10.1016/j.palaeo.2020.110027
Received 23 February 2020; Received in revised form 2 September 2020; Accepted 10 September 2020
Available online 18 September 2020
0031-0182/

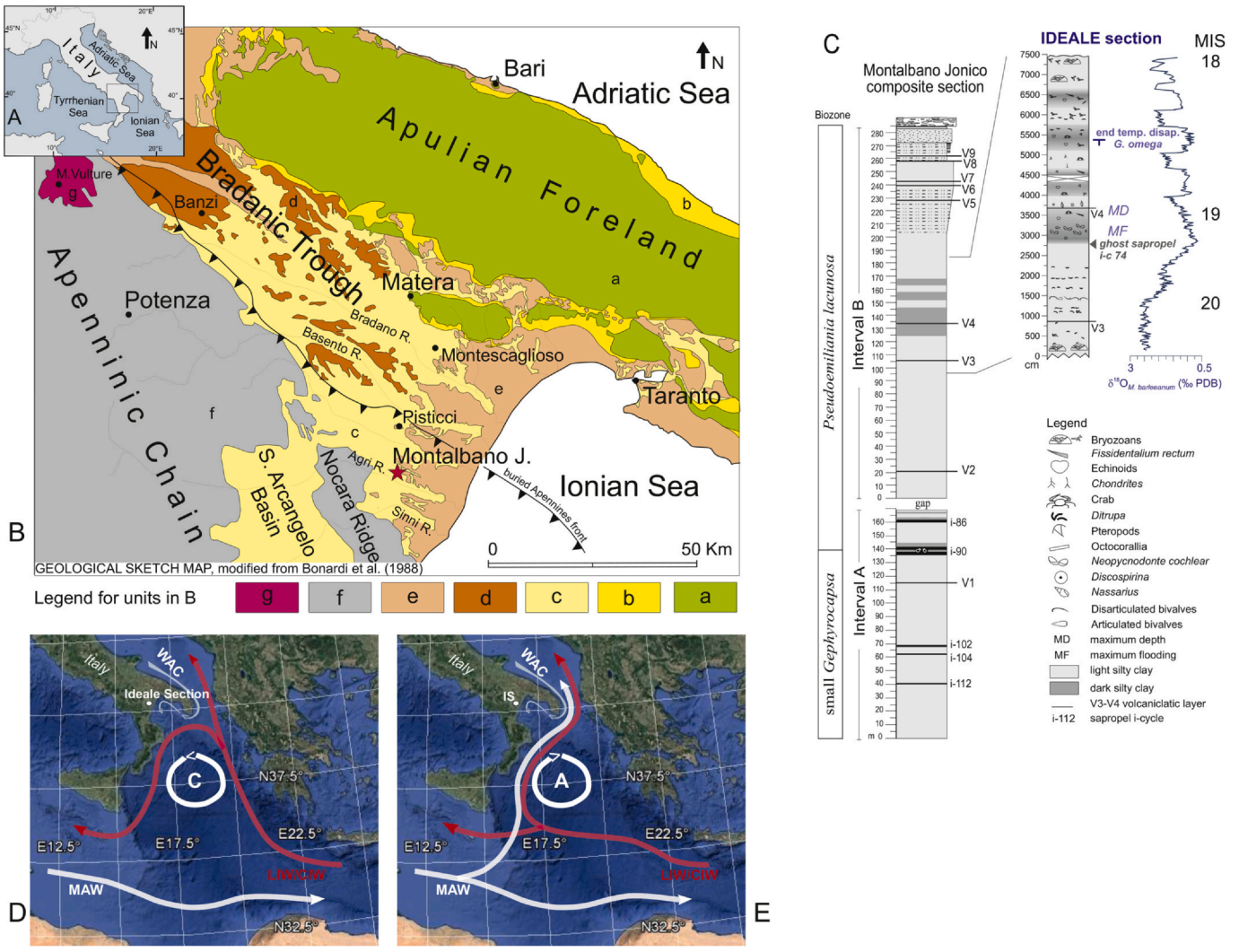

Fig. 1. A: location of the study area. B: simplified regional geological setting of southern Italy. Red star indicates the location of the Montalbano Jonico section. Legend of the geological map in fig. B: a) Cretaceous units of the Apulian Foreland; b) Calcareous units of the Plio-Pleistocene Apennines Foreland; c) Siliciclastic units of the Plio-Pleistocene Apennines Foreland; d) Lower Pleistocene regressive conglomerates of the Bradanic Trough; e) Middle-Upper Pleistocene marine terraced deposits of the Bradanic Trough; f) Triassic-Neogene units of the Apennines Chain; g) Quaternary volcanic units. C: main lithological features of Montalbano Jonico composite section (Intervals A and B), with details on paleontological and oxygen isotope data at the Ideale section (Ciaranfi et al., 2010; Maiorano et al., 2010; Nomade et al., 2019). MD: maximum depth; MF: maximum flooding; i-cycle 74: ghost sapropel associated with insolation cycle 74. The end of temporary disappearance of *Gephyrocapsa omega* is also shown on the Ideale section. D-E: main sea surface and subsurface water currents and decadal-scale cyclonic (D) and anticyclonic (E) circulation in the Ionian Sea, redrawn according to Gačić et al. (2010) (see text for details). MAW: modified Atlantic water; LIW/CIW: Levantine/Cretan intermediate waters; WAC: Western Adriatic current. (For interpretation of the references to colour in this figure legend, the reader is referred to the web version of this article.)

variability that is evidenced by the partition in substages a, b, and c in the $\delta^{18}O$ oscillations (Railsback et al., 2015), associated with 19.3, 19.2, and 19.1 events (Bassinot et al., 1994). They may have relevant implications in climatostratigraphy (Miller and Wright, 2017), coherently with the wide use of oxygen isotope signature for Quaternary chronostratigraphic subdivision. Specifically, the Lower-Middle Pleistocene chronostratigraphic boundary, close to the Matuyama-Brunhes paleomagnetic reversal, is associated worldwide with the MIS 19c/MIS 19b transition at ~773 ka (Head, 2019, and reference therein). A distinct occurrence of the first climate deterioration marked by MIS 19b and climate oscillations in MIS 19a, have been revealed by recent high-resolution proxies in several marine (Kleiven et al., 2011; Tzedakis et al., 2012; Emanuele et al., 2015; Ferretti et al., 2015; Sánchez Goñi et al., 2016; Nomade et al., 2019; Toti et al., 2020), lacustrine sediments (Giaccio et al., 2015; Regattieri et al., 2019), and ice core (e.g. Pol et al., 2010).

These climate episodes, occurring at a wide scale (Nomade et al., 2019), may have not been given coherent chronologies, possibly due to different age-model strategies and the fact that different proxies may have been used to identify them. This makes it difficult to correlate climate stages and events with accuracy and to interpret climate dynamics and temporal relationship (ie. lead/lag) between high and mid latitudes or between marine and terrestrial realms, thus preventing the comprehension of cause-effect connections and the climate propagation of changes at regional and global scale.

The on land marine Ideale section (IS), as part of the Montalbano Jonico section (MJS, southern Italy) encompassing MIS 37-MIS 16, offers the opportunity to improve the paleoclimate framework of MIS 19 due to its high sedimentation rate and environmental setting. The IS deposited in lower circalittoral-upper bathyal setting, not far from a peninsular coastline, and thus registered even slight climatically induced modifications such as changes in sea level, precipitation, and inorganic/organic input from land. Such a marine environment is also suitable to provide numerous proxy data, in the form of planktonic and

benthic foraminifera, coccolithophores, and marine biomarkers. The IS has been extensively studied in recent years due to its potential to represent the Lower-Middle Pleistocene chronostratigraphic boundary (e.g. Ciaranfi et al., 2010; Maiorano et al., 2010, 2016a; Bertini et al., 2015; Marino et al., 2015, 2016; Petrosino et al., 2015; Simon et al., 2017; Nomade et al., 2019). Short-term climate episodes in the latest MIS 20 and Termination IX (TIX) have been referred to Heinrich-like (Ht), Bølling-Allerød-like (BAt), and Younger-Dryas like (YDt) based on multi-proxy investigation thus suggesting a climate variability comparable to that documented during the last deglaciation (Maiorano et al., 2016a). The latter authors suggested the need of higher resolution data-set to support these evidences in a finer constrained time frame. The more recent, very high-resolution benthic (*Cassidulina carinata*, *Melonis barleeanum*) $\delta^{18}O$ and $\delta^{13}C$ records (Nomade et al., 2019) have improved the chronology of the IS, detailing the pattern of MIS 19 substages and the three interstadial phases in MIS 19a (19a-1, 19a-2, and 19a-3), highlighting the centennial-scale timing of these climate oscillations and their worldwide correlability. A sapropel-like layer has been recognized in the early MIS 19 (Maiorano et al., 2016a; Nomade et al., 2019) and associated with insolation-cycle (i-cycle) 74 (784 ka, Lourens, 2004; 785 ka, Konijnendijk et al., 2014).

In the present work we present new high-resolution alkenone-SST data-set acquired at the IS, representing the first one recorded in the Mediterranean Sea for the time interval spanning MIS 20-MIS 18. New quantitative calcareous plankton (coccolithophores and foraminifera) results, obtained on the same samples used for marine biomarkers and for the isotopic study of Nomade et al. (2019), are also presented, providing a paleoecological window into synchronous marine response to major environmental modifications. The combination of this new data-set with the detailed benthic isotope records available at the IS provides useful insights into i) the marine surface/subsurface water conditions in the central Mediterranean during an important interglacial of mid-Pleistocene transition considered the best analogue of the current interglacial (Holocene), ii) the terminal stadial event in late MIS 20 and its oceanographic-atmospheric connection with North Atlantic climate, iii) the high-frequency climate variability across TIX, making it possible to better address its apparent similarity with the rapid variability that occurred during TI. The comparison of new data with selected high-resolution climate references from North Atlantic Ocean provides additional highlights on central Mediterranean response to local or global climate via atmospheric-oceanographic processes.

2. Oceanography

Sediments of the MJS were deposited in the paleo Gulf of Taranto (Fig. 1D), in the north Ionian Sea. At this location important detrital sediment supply derives mainly from Apennines rivers (Goudeau et al., 2013). Sediments from the Po River and other Apennines rivers may also arrive in the eastern Gulf of Taranto through the Western Adriatic Current (WAC) (Fig. 1D). This river-diluted (salinity about 37 psu) nutrient-rich current flows southward along the southern Italian coast in a narrow coastal band from the northern Adriatic Sea, and mixes with the more saline Ionian waters (up to 39.5 psu in the central Ionian Sea) (Poulain, 2001; Bignami et al., 2007; Turchetto et al., 2007; Grauel and Bernasconi, 2010). The WAC has higher influence in winter and spring (Poulain, 2001) than in summer and is characterized by significant inter-annual variability (Milligan and Cattaneo, 2007). In the Gulf of Taranto, the highly saline Levantine Intermediate Water (LIW), flowing from the central Ionian Sea, may be recorded at the water depth of 200–600 m (Savini and Corselli, 2010). The Northern Ionian Gyre (NIG) that has decadal scale cyclonic (Fig. 1D) and anticyclonic phases (Fig. 1E) (Civitarese et al., 2010) characterizes the central open ocean area of the Gulf of Taranto. The cyclonic phase (Fig. 1D) is characterized by saltier Levantine/Cretan Intermediate Waters (LIW/CIW) that flow northward into the Adriatic, while anticyclonic phase (Fig. 1E) records advection of less saline Ionian water diluted by Modified Atlantic Waters (MAW) (Civitarese et al., 2010). In the first case poor-nutrient LIW/CIW waters enter the north Ionian Sea and south Adriatic Sea, while the influx of MAW during anticyclonic phase favours upwelling events and nutrients supply at the periphery of the anticyclonic NIG along the southern Italian coasts before reaches the south Adriatic Sea (Civitarese et al., 2010). The alternating anticyclonic and cyclonic states are known as Adriatic-Ionian bimodal oscillation system (Civitarese et al., 2010; Gačić et al., 2010) that may influence nutrient distribution and phytoplankton growth (Civitarese et al., 2010; Batistić et al., 2017). Modern annual mean SSTs in the Gulf of Taranto are about 19.7 °C (Pujol and Vergnaud-Grazzini, 1995). During summer, they vary from 26 °C to 15 °C at the surface and at 50 m depth, respectively, and the water column is stratified (Zonneveld et al., 2008; Grauel and Bernasconi, 2010). During winter, SSTs vary between 13 °C and 15 °C. These seasonal temperature changes may affect the upper 100 m of the water column (Socal et al., 1999; Locarnini et al., 2010).

Today, the high latitude North Atlantic and Arctic climate perturbations rapidly spread to the northern hinterlands of the Mediterranean and are channelized in mountain valleys through intense northerly flows of cold and dry air masses ('Mistral', 'Bora', 'Vardar' winds) over the northwestern Mediterranean, the Adriatic and the Aegean basins (Mariolopoulos, 1961; Leaman and Schott, 1991; Poulos et al., 1997). These polar and continental winter airflows cause intense evaporation and cooling of the sea surface and terrestrial vegetation (e.g., Leaman and Schott, 1991; Saaroni et al., 1996; Poulos et al., 1997; Maheras et al., 1999; Casford et al., 2003; Rohling et al., 2009).

3. Geological setting and stratigraphy

The IS, as part of the Montalbano Jonico succession (MJS), crops out in the south-western margin of the Bradanic Trough, at about 16 km inland from the Ionian Coast (40°17′29.52" N 16°33'10.58"E) (Fig. 1B). The Bradanic Trough (e.g. Casnedi, 1988), located between the Apennines Chain to the west and the Apulian foreland eastward (Fig. 1B), is a foredeep basin of the post-Messinian Apennines. Its origin and evolution are associated with the eastward roll-back of the subduction hinge of the Apulia platform and the evolution of the external Apennines thrust front during the Plio-Pleistocene (e.g., Patacca and Scandone, 2007 and references therein). The foredeep was characterized by high rates of subsidence until the Calabrian, after which it underwent a diachronous uplift starting from the Genzano-Banzi area during late Calabrian and proceeding southeastward to the actual Ionian coast by Holocene time. In the late Calabrian, the central sector of the Bradanic Trough emerged while the southern sector, where the study section is located, was still subsiding. The central foredeep sector reached its maximum deepening in the Early-Middle Pleistocene (e.g., Maiorano et al., 2016a). From the Middle Pleistocene, the sedimentation reveals a shoaling-upward trend due to the uplift of the area (uplift rate of 0.1–0.5 mm/years, e.g. Doglioni et al., 1996) that led to the emersion of the area since 0.6/0.7 Ma. Regionally, the gradual emersion of the area is testified by several continental and marine terraces, represented by transitional and continental deposits of ancient alluvial and costal plains developed between 0.7 Ma and the Late Pleistocene (e.g. Vezzani, 1967; Brückner, 1980a, 1980b; Pescatore et al., 2009; Sauer et al., 2010; Boenzi et al., 2014).

The MJS (Fig. 1C) belongs to the argille subapennine informal unit (Azzaroli et al., 1968), representing its middle-upper portion, Early to Middle Pleistocene in age (Ciaranfi et al., 2010). It consists of coarsening-upwards deposits ranging from silty clays to silty sands and includes nine tephra layers (V1-V9) (Fig. 1C). The tephra layers (V1-V9) were chemically and mineralogically characterized and correlated to analogous layers from south-central Italy lacustrine and marine successions, within a Lower-Middle Pleistocene Mediterranean tephrostratigraphic frame (Petrosino et al., 2015). The MJS, in its lower part, includes five dark horizons interpreted as sapropel layers (D'Alessandro et al., 2003; Stefanelli, 2004; Stefanelli et al., 2005;

Maiorano et al., 2008) and correlated, from oldest to youngest, to insolation cycles i-112, i-104, i-102, i-90, and i-86, based on the Mediterranean sapropel stratigraphy of Lourens (2004) and Lourens et al. (2004). The calcareous nannofossil biostratigraphy indicates that the entire succession belongs to the small *Gephyrocapsa* and *Pseudoemiliania lacunosa* zones, based on the biostratigraphic scheme of Rio et al. (1990) (Fig. 1C). Several deepening-shallowing cycles, from bathyal to circalittoral environments, have been recognized based on micro- and macro-invertebrate benthic assemblages (D'Alessandro et al., 2003; Stefanelli, 2003; Ciaranfi and D'Alessandro, 2005; Girone, 2005). Specifically, benthic paleocommunities from the lower part of succession (Interval A) indicated upper slope environments, with a maximum depth of ca. 500 m, while paleocommunities of upper portion (Interval B) pointed out to outer to inner shelf settings with short-term deepening towards upper slope.

The IS, in Interval B, consists of clays and silty clays bracketed by two tephra layers, V3 and V4. The V3 and V4 layers were radiometrically dated and their $^{40}Ar/^{39}Ar$ ages are 801.2 ± 19.5 ka (Maiorano et al., 2010), 773.9 ± 1.3 ka (Petrosino et al., 2015), respectively. The V3 tephra is located within the MIS 20 interval (at 820 cm) and V4 is at the transition from MIS 19c to MIS 19b (at 3660 cm) (Fig. 1C). Due to its high stratigraphic value in constraining the MIS 19c/19b transition, coincident with the $^{10}Be/^{9}Be$ peak interpreted as the Earth magnetic field collapse during the Matuyama-Brunhes reversal (Simon et al., 2017), V4 has been re-dated at the LSCE laboratory (France). New dating provided an $^{40}Ar/^{39}Ar$ age of 774.1 ± 0.9 ka (Nomade et al., 2019), which is in good agreement with the Ar/Ar age estimate of Petrosino et al. (2015). A shallow-water analogue of the "red interval" ("ghost sapropel", oxidized sapropel, Emeis et al., 2000a), i-cycle 74 (784 ka, Lourens, 2004; 785 ka, Konijnendijk et al., 2014) has been indicated by Maiorano et al. (2016a) in the early MIS 19 based on multidisciplinary approach, and also supported by Nomade et al. (2019) based on the very low values in $\delta^{13}C_{C.carinata}$ in the interval from 2620 to 2840 cm (Fig. 1C). Upwards, the dark grey bands in the IS (Fig. 1C) correspond to higher kaolinite and smectite content and increased chemical weathering on land (Maiorano et al., 2016a); the clay fraction increases significantly (20–31%, average 24%) from the onset of MIS 19 upwards, although several fluctuations have been observed through the interval encompassing MIS 19a towards MIS 18. In contrast, the light grey bands are related to increases of quartz and dolomite associated with enhanced supplies of the coarser detrital mineral components into the basin (Maiorano et al., 2016a). Dark and light intervals correspond to lower (interglacial, interstadials) and higher (glacial, stadials) benthic $\delta^{18}O$ values, respectively, suggesting the glacio-eustatic/climate control on sedimentary features of the IS. However, the influx of fresh water of on land origin during wetter climate was not excluded during lighter $\delta^{18}O$ and darker sedimentation phases, in contrast to more arid climate during heavier $\delta^{18}O$ intervals (Bertini et al., 2015; Nomade et al., 2019). The shallowing-deepening cycles through MIS 20–18 are also highlighted by marine micro- and macrobenthic assemblages (D'Alessandro et al., 2003; Stefanelli, 2003; Aiello et al., 2015), and pollen distality index (Bertini et al., 2015). In detail, paleodepths range from about 100 m to 180–200 m (Aiello et al., 2015) which implies a water column mainly distributed in the photic zone. A maximum flooding in the mid MIS 19c (MF, Fig. 1C) followed by the maximum depth interval (MD, Fig. 1C) are documented by D'Alessandro et al. (2003) based on the benthic macro-invertebrate communities.

4. Methods

Samples were collected from unaltered sediments by removing the surficial weathered rind. Alkenones and calcareous plankton assemblages were investigated in 170 and 167 samples, respectively, from the same levels analyzed for the high-resolution isotope curves of Nomade et al. (2019). The sample spacing is between 20 and 40 cm and corresponds to a temporal resolution of 200 years in MIS 20, down to about 100 years during selected intervals (mainly Termination IX and MIS 19a), according to the age-model of Nomade et al. (2019).

4.1. Biomarker analyses

Lipid biomarker extractions were carried out on 5 g freeze-dried, ground samples by accelerated solvent extraction (Dionex ASE-200) at Brown University. The complexity of interfering peaks in the region where C_{37} and C_{38} alkenones elute via gas chromatography (GC) required purification by silica gel flash column chromatography prior to GC analysis. Gas chromatography was carried out on an Agilent (60 m, DB-1 column) with the following parameters: initial temperature 90 °C, increased to 255 °C with 40 °C/min rate, increased by 1.5 °C/min to 300 °C, increased by 10 °C/min to 320 °C, and an isothermal hold at 320 °C for 11 min. GC performance was monitored by running a lab standard extract at the beginning and end of each run, and running replicates ("bookends") of IS extracts within the run to rule out chromatographic drift. In addition to the $U^{k'}_{37}$ index, we determined comparable C_{38} unsaturation indices for quality control; the signal noise of these determinations was less than for the $U^{k'}_{37}$ index, but they served a redundancy checks that would have indicated the presence of outliers possibly indicating compounds interfering with alkenones in GC analysis. Reproducibility was ~0.01 $U^{k'}_{37}$ units and ~ 5% relative error for C_{37} total. The total C_{37} (μg/g of dry weight sediment) is the sum of $C_{37:2}$ and $C_{37:3}$ alkenones. For this work we followed the calibration of Müller et al. (1998) to translate $U^{k'}_{37}$ to SST.

4.2. Microfossils

Analyses for planktonic foraminifera were carried out on the residue > 150 μm after the sediment was dried and washed on a 63 μm sieve. The residues were split until a representative aliquot, containing about 300 specimens, has been obtained. The species abundances were quantified as percentages on the total number of planktonic foraminifers. Sixteen species or species groups were distinguished: *Globigerinoides ruber* includes morphotype *Globigerinoides ruber* white, and *Globigerinoides elongatus* (sensu Aurahs et al., 2011); *Trilobatus sacculifer* includes *Trilobatus trilobus*, *Trilobatus sacculifer* and *Trilobatus quadrilobatus* (sensu Hemleben et al., 1989; André et al., 2013; Spezzaferri et al., 2015). The SPRUDTS group (sensu Rohling et al., 1993) (*Globigerinella siphonifera*, *Hastigerina pelagica*, *Globoturborotalita rubescens*, *Orbulina universa*, *Beella digitata*, *Globoturborotalita tenella*, and *T. sacculifer*) and *G. ruber* were grouped as warm water indicators (foram-wwt). The criteria adopted for the taxonomy of *Neogloboquadrina* spp. are from Darling et al. (2006): *Neogloboquadrina incompta* corresponds to neogroboquadrinids previously referred to *N. pachyderma* (dextral) and includes intergrades between *N. pachyderma* (dextral) and *N. dutertrei*; *N. pachyderma* includes the left coiling specimens. It is a polar-subpolar taxon in the Northern Hemisphere (Bé and Tolderlund, 1971; Hemleben et al., 1989; Johannessen et al., 1994; Simstich et al., 2003; Darling et al., 2006) and has been found rare (< 5%) in central and eastern Mediterranean Sea during Pleistocene (e.g. Thunell, 1978; Rohling and Gieskes, 1989; Rohling et al., 1993; Hayes et al., 1999, 2005; Sprovieri et al., 2003, 2012; Triantaphyllou et al., 2009; Siani et al., 2010). Increases in the abundance of *N. pachyderma* has been used as a proxy of Atlantic cold (melt) water influx into Mediterranean (Hemleben et al., 1989; Pérez-Folgado et al., 2003; Sierro et al., 2005; Girone et al., 2013; Capotondi et al., 2016; Marino et al., 2018). *N. incompta* is a cold and eutrophic taxon, indicative of deep chlorophyll maximum at the base of the euphotic layer (Hemleben et al., 1989; Reynolds and Thunell, 1986; Pujol and Vergnaud-Grazzini, 1995; Rohling et al., 1995). *G. bulloides*, due to its opportunistic behavior, has been used as an indicator of high-nutrient content, the species preferring eutrophic condition related to upwelling, strong seasonal mixing or river input (Tolderlund and Bé, 1971; Hemleben

et al., 1989; Pujol and Vergnaud-Grazzini, 1995; Rohling et al., 1997; Bárcena et al., 2004; Geraga et al., 2005, 2008). *G. inflata* has been used a proxy of cool-temperate waters, deep pycnocline, and ventilated conditions (Hemleben et al., 1989; Pujol and Vergnaud-Grazzini, 1995; Rohling et al., 1995; Bárcena et al., 2004).

Slides for coccolithophore analysis were prepared according to Flores and Sierro (1997) to estimate absolute coccolith abundances. Quantitative analyses were performed using a polarized light microscope at 1000× magnification and abundances were determined by counting at least 500 coccoliths of all sizes, in a varying number of fields of view. Species abundances were expressed as percentage and as N (number of coccoliths/g of sediment). The warm-water taxa *Umbilicosphaera sibogae* s.l., *Calciosolenia* spp., *Discosphaera tubifera*, *Rhabdospaera clavigera*, *Umbellosphaera* spp., *Oolithotus* spp., *Helicosphaera pavimentum* were grouped together (nanno-wwt) according to their ecological preferences and their higher abundances during warmer and oligotrophic conditions (McIntyre and Bé, 1967; Winter et al., 1994; Ziveri et al., 2004; Baumann et al., 2004; Boeckel and Baumann, 2004; Saavedra-Pellitero et al., 2010; Palumbo et al., 2013; Maiorano et al., 2015; Marino et al., 2018; Trotta et al., 2019; Toti et al., 2020). *Coccolithus pelagicus* ssp. *pelagicus*, a subarctic taxon (Baumann et al., 2000; Geisen et al., 2002), was used as an indicator of cold meltwater influx in mid-latitude North Atlantic Ocean (Parente et al., 2004; Marino et al., 2011, 2014; Amore et al., 2012; Maiorano et al., 2015), even in Mediterranean basin (Girone et al., 2013; Maiorano et al., 2016a; Marino et al., 2018; Trotta et al., 2019; Toti et al., 2020). Increases of *Florisphaera profunda* that thrive in the lower photic zone were considered indicative of deep nutricline (Molfino and McIntyre, 1990). The taxon may also inhabit surface water when turbidity and low light occur due to too high surface detrital input and low light intensity (Ahagon et al., 1993; Colmenero-Hidalgo et al., 2004; Maiorano et al., 2008, 2016a; Girone et al., 2013). Taxonomy of gephyrocapsids follows the criteria of Maiorano et al. (2013). *Helicosphaera carteri* has been used as a proxy of enhanced detrital input, surface water turbidity and low salinity (Colmenero-Hidalgo et al., 2004), conditions associated with higher runoff and enhanced nutrients (Bonomo et al., 2018) or cold glacial phases and low sea level in Mediterranean Sea (Weaver and Pujol, 1988; Colmenero-Hidalgo et al., 2004; Maiorano et al., 2013, 2015, 2016b; Marino et al., 2018).

5. Results

At the IS, SST pattern records values between 12 and ~ 22 °C (Fig. 2D). The lowest SSTs characterize the lower part of the studied section (MIS 20), substage MIS 19b and the stadial episodes in MIS 19a. On the other hand, higher temperatures are recorded in MIS 19c and interstadials 19a-1, 19a-2, and 19a-3 (Fig. 2D). Calcareous plankton key taxa used here for paleoenvironmental reconstruction show relevant fluctuations through time. Total coccoliths (tot N, Fig. 2F) present abundances mainly lower than 20 coccoliths/g (x 10^7) in MIS 20 and during TIX, and lower than 30 coccoliths/g (x 10^7) from MIS 19b towards the end of the studied section, with slight increases up to 40 coccoliths/g (x 10^7) during interstadials in MIS 19a. Total N records higher values, up to 100 coccoliths/g (x 10^7), during MIS 19c. Coccolithophore wwt (nanno wwt, Fig. 2G), although low in abundance throughout the section, shows fluctuating increases in MIS 19c and interstadial 19a-2, with abundance never higher than 0.5 coccoliths/g (x 10^7). The abundance of *F. profunda* generally is lower that 1 coccoliths/g (x 10^7) while it shows major fluctuating increase up to 3.2 coccoliths/g (x 10^7) in MIS 19c (Fig. 3F). *Syracosphaera* spp. are a minor component of coccolithophore assemblage (Fig. 3G), however they record a distinct abundance peak of 0.5 coccoliths/g (x 10^7) in the lower MIS 19c. The relative abundances of planktonic foraminifera wwt (Fig. 2H) vary between 5 and 80% and depict glacial-interglacial and stadial-interstadial episodes with a few short-term minor increases during TIX. In particular, the relative abundances of *T. sacculifer* reach 3.5% in MIS 19c and MIS 19a-2 interstadial (Fig. 2H); *G. ruber* is a significant component reaching relative abundances up to 72% mainly starting from MIS 19c upwards (Fig. 3D). The polar-subpolar *C. pelagicus* ssp. *pelagicus* and *N. pachyderma* are more abundant, with values up to 22% and 5%, respectively, in MIS 20, during TIX and in MIS 19b as well as in colder phases of MIS 19a (Fig. 2 K-L). *H. carteri* shows a comparable pattern (Fig. 2M) with fluctuating relative abundances lower than 7.5%. *N. incompta* has discontinuous relative abundance, with peaks up to 17% in MIS 20 and TIX, in lower MIS 19c, and in short-term intervals of MIS 19a, while it is absent in the upper MIS 19c (Fig. 2I). *G. bulloides* is continuously present throughout the IS and shows variable abundances, which seem to increase in the upper portion of IS (Fig. 2J). *G. inflata* records higher abundances, up to 80%, in distinct periods of TIX and in the stadials of MIS 19a, whereas it is absent in MIS 19c and interstadial phases (Fig. 2N). *O. universa* shows abundance variations during the investigated interval, with more prominent peaks, up to 27%, in selected short-term intervals of TIX and in MIS 19a interstadials.

6. Discussion

Results are discussed starting from the lower portion of the studied record upwards, focusing on environmental changes occurred in late MIS 20 and TIX (Fig. 2) to MIS 19 onset (Figs. 2-3), and towards MIS 19b-19a, and MIS 18 beginning (Fig. 2). Comparisons with climate proxies from other extra-Mediterranean reference sections are presented in Fig. 4.

6.1. Environmental changes through late MIS 20: the terminal stadial event Med-H_{TIX}

Between 794 and 788.5 ka, a terminal stadial event (sensu Hodell et al., 2015), hereafter named Med-H_{TIX}, may be recognized, primarily based on the SST decreases (Fig. 2D) and the polar-subpolar *N. pachyderma* and *C. pelagicus* ssp. *pelagicus* increase (Fig. 2 K-L). In more details, SSTs were at least 4–5 °C cooler than pre-Med-H_{TIX} (17–21 °C) with fluctuating values mainly below 16 °C, and minimum at 13 °C. These values are compatible with Δ^{47}-derived subsurface temperature of 12.1 °C measured on benthic foraminifera at 794 ka (Peral et al., 2020). *C. pelagicus* ssp. *pelagicus* and *N. pachyderma* increase from percentages mainly below 3% and 10%, to values up to 5% and 20%, respectively. The concomitant low abundances of the coccolithophore and planktonic foraminifera wwt (Fig. 2 G-H) are coherent with colder sea surface water conditions in the basin linked to Med-H_{TIX}, lasting about 5 kyr at the IS. The pollen assemblages at the IS indicated a synchronous large expansion of open landscapes including prevalent (cold) dry steppes on land (Bertini et al., 2015).

6.1.1. Oceanographic and atmospheric processes during terminal stadial Med-H_{TIX}

The decreasing trend of temperature in latest MIS 20 is accompanied by a similar pattern of benthic $\delta^{13}C$ (Fig. 2P), the latter suggesting an increasing trend of water column stratification. The lightening of 1‰ in the $\delta^{18}O_{M.\ barleeanum}$ record during Med-H_{TIX} event (Fig. 2C) could reflect the influx of lighter fresh water at the site location, possibly affecting oxygen isotope composition of bottom water and benthic *Melonis barleeanum* tests. The question remains whether the benthic $\delta^{18}O$ signal reflects (i) a sea-surface signal, owing to the shallow depositional environment of IS (~ 100 m, Aiello et al., 2015) during low sea level glacial phase (Fig. 2B), or (i) a sub-surface lateral advection signal.

The first hypothesis, i.e. the occurrence of cold and fresher surface waters at the location of IS, may point towards the arrival of melt waters coming from mountain glaciers of the close hinterland (Alpine and Apennines chains), as during the last termination (Maselli et al., 2011). Alternatively, or concurrently, fresher water lateral inflow into

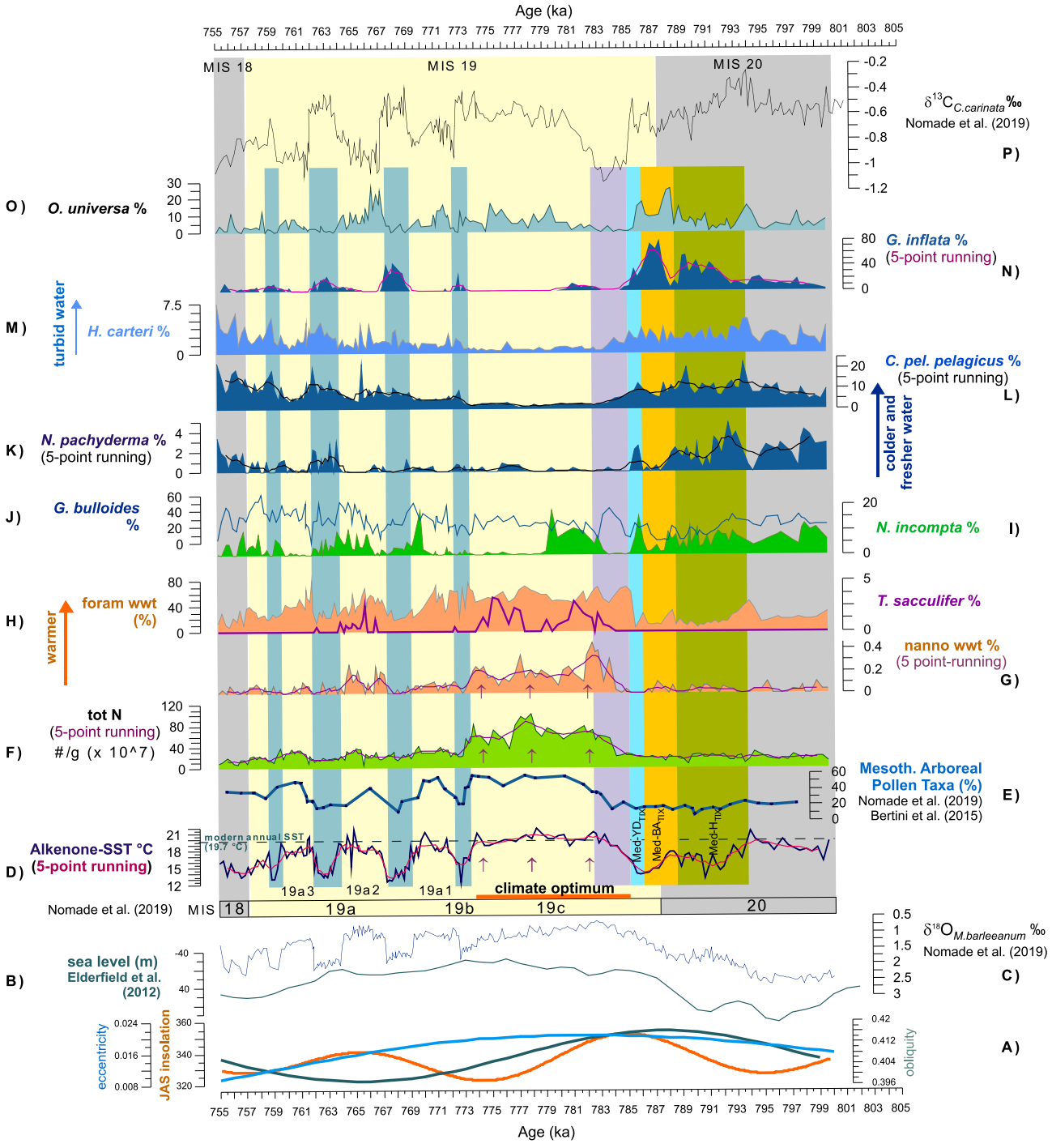

Fig. 2. Quantitative abundance patterns of selected calcareous plankton taxa (F-O) expressed as percentage, alkenone-SST (D), and benthic oxygen (C) and carbon (P) isotope records at the Ideale section. Foram wwt (H) and Nanno wwt (G) curves are planktonic foraminifera and calcareous nannofossil warm water taxa, respectively; tot N (F) (number of coccoliths/g of sediment, #/g), is the total abundance of coccoliths. Modern annual SST (19.6 °C) is shown on alkenone-SST record according to Pujol and Vergnaud-Grazzini (1995). A: mean summer insolation (JAS), obliquity and eccentricity (65° N) from Laskar et al. (2004). B: sea level curve Elderfield et al. (2012); 19a1-19a3 are interstadial phases during 19a according to Nomade et al. (2019). Stage boundaries and climate optimum are marked according to Nomade et al. (2019). Glacial MIS 20 and MIS 18 intervals are evidenced by grey bands. Light yellow color marks interglacial/interstadial phases. Light blue bands on proxy records are stadial phases; green, dark yellow, blue bands represent Med-H_{TIX}, Med-BA_{TIX}, Med-YD_{TIX}, respectively. Lilac band is the ghost sapropel interval according to Maiorano et al. (2016a) and Nomade et al. (2019). Purple arrows indicate the main phases of ameliorated climate conditions in MIS 19c. (For interpretation of the references to colour in this figure legend, the reader is referred to the web version of this article.)

the Ionian Sea may have occurred through the Gibraltar Strait in association with North Atlantic ice melting, such a scenario being coherent to what has been observed in the western Mediterranean during recent glacial stadials correlated to Heinrich event in North Atlantic (e.g. Cacho et al., 1999, 2000; Sierro et al., 2005; Frigola et al., 2008; Martrat et al., 2014).

The occurrence of the Med-H_{TIX} in late MIS 20 is not only observed in IS but is also supported by data from the Balearic Sea (Quivelli, 2020). These data indicate cold fresh water inflow from Atlantic or surrounding mountain glacier during the terminal stadial of MIS 20,

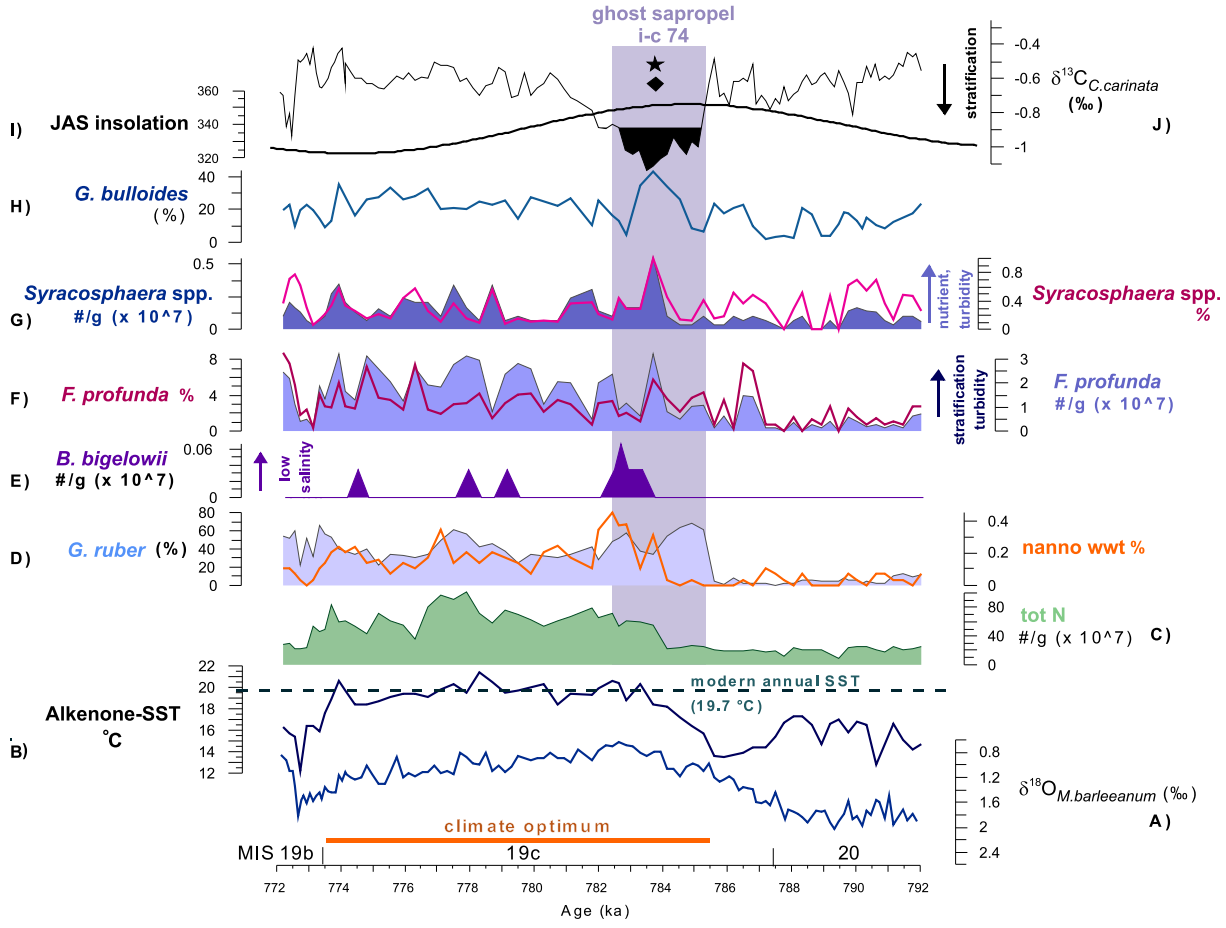

Fig. 3. Quantitative abundance patterns of selected calcareous plankton taxa (C-H) expressed as percentage and/or as number of coccoliths/g of sediment (#/g), alkenone-SST (B), and benthic oxygen (A) and carbon (J) isotope records at the Ideale section. Tot N (C) is the total abundance of coccoliths. Lilac band represents the interval of ghost sapropel i-c 74 according to Maiorano et al. (2016a) and Nomade et al. (2019). Star symbol in the sapropel interval is the acme occurrence of dinocyst *Polysphaeridium zoharyi* (Bertini et al., 2015; Maiorano et al., 2016a), that has been associated with Mediterranean sapropel formation (Giunta et al., 2006; Sangiorgi et al., 2006); diamond symbol in the sapropel interval is the increase episode of benthic foraminifera infauna/epifauna ratio (Stefanelli, 2003) as signal of stressed condition at the sea bottom (Marino et al., 2015). I: mean summer insolation (JAS 65° N) from Laskar et al. (2004). Stage/substage boundaries and climate optimum are marked according to Nomade et al. (2019).

based on the increase of polar-subpolar *N. pachyderma* and lower alkenone-derived SST (between 8 and 11 °C), together with a prominent lightening of planktonic $\delta^{18}O$. Similarly, lighter planktonic $\delta^{18}O$ values and changes in the calcareous plankton assemblages suggest the arrival of Atlantic water in the central Mediterranean during main terminations of the last 70 ka (Sprovieri et al., 2012; Incarbona et al., 2013). As far as IS benthic $\delta^{18}O$ is concerned, evaluating the respective contribution of ice-sheet volume signal or local freshwater input during late MIS 20 cannot be assessed here since it would require additional proxies, and this is far from the aim of this work. Additionnal studies are mandatory to decipher between the different hypotheses.

The occurrence of Med-H_{TIX} has a close temporal relationship with the deposition of ice rafted debris (IRD) in the North Atlantic where low $\delta^{13}C_{benthos}$ values at the sites 980 (Wright and Flower, 2002) and 983 (Kleiven et al., 2011) (see Fig. 4 P-S), are suggestive of water column stratification and shutdown of Atlantic Meridional Overturning Circulation (AMOC) (Ganopolski and Rahmstorf, 2001). There is no evidence of IRD at the mid-latitude Iberian margin, a sensitive area that recorded IRD occurrence during colder episodes of the mid-Pleistocene glacials (Stein et al., 2009; Voelker et al., 2010; Rodrigues et al., 2011). Recently, clear indications of low salinity and cold melt water inflow during late MIS 20 have been documented in that area, at the Site U1385, based on low alkenone-SST (between 12 and 9 °C, Fig. 4N) and higher $C_{37:4}$ (Fig. 4M) (Rodrigues et al., 2017), and a peak of *N. pachyderma* (Martin-Garcia et al., 2015), as a signal of southward migration of Polar Front. At the same time, the minima in $\delta^{13}C_{benthos}$ (Fig. 4L) and in log Ca/Ti patterns at the Iberian margin U1385 core (Fig. 4K) (Hodell et al., 2015) point to North Atlantic low bottom water ventilation, due to reduced North Atlantic Deep Water formation (Raymo et al., 1990, 1997), and the occurrence of a cold stadial. We suggest that the Med-H_{TIX} in the late MIS 20 at the IS is coherent with the contemporaneous oceanographic and climate signals at the southwestern Iberian margin and northern Atlantic (Fig. 4). These evidences imply a clear Mediterranean response to high latitude North Atlantic climate change through oceanographic connection during mid-Pleistocene stadials.

The slightly warmer temperatures at the IS, compared to those recorded at the same time in the southwestern Iberian margin (Fig. 4N) and Balearic basin (8–11 °C; Quivelli, 2020), may be a result of the west-east SST (and salinity) increase of MAW during its eastward route in the Mediterranean (Béthoux, 1979; Malanotte-Rizzoli et al., 1999, 2014; von Grafenstein et al., 1999; Pinardi and Masetti, 2000). Similar temperature gradient from west (Alboran Sea, ~10–11 °C, Cacho et al., 2001; Martrat et al., 2014) to east (Tyrrhenian Sea, 11–14 °C, Paterne et al., 1999; eastern Mediterranean, 14–16 °C, Castañeda et al., 2010) was also recorded during H1.

The cold climate frame reconstructed for the Med-H_{TIX} based on our marine proxies may have been also controlled by Atlantic-

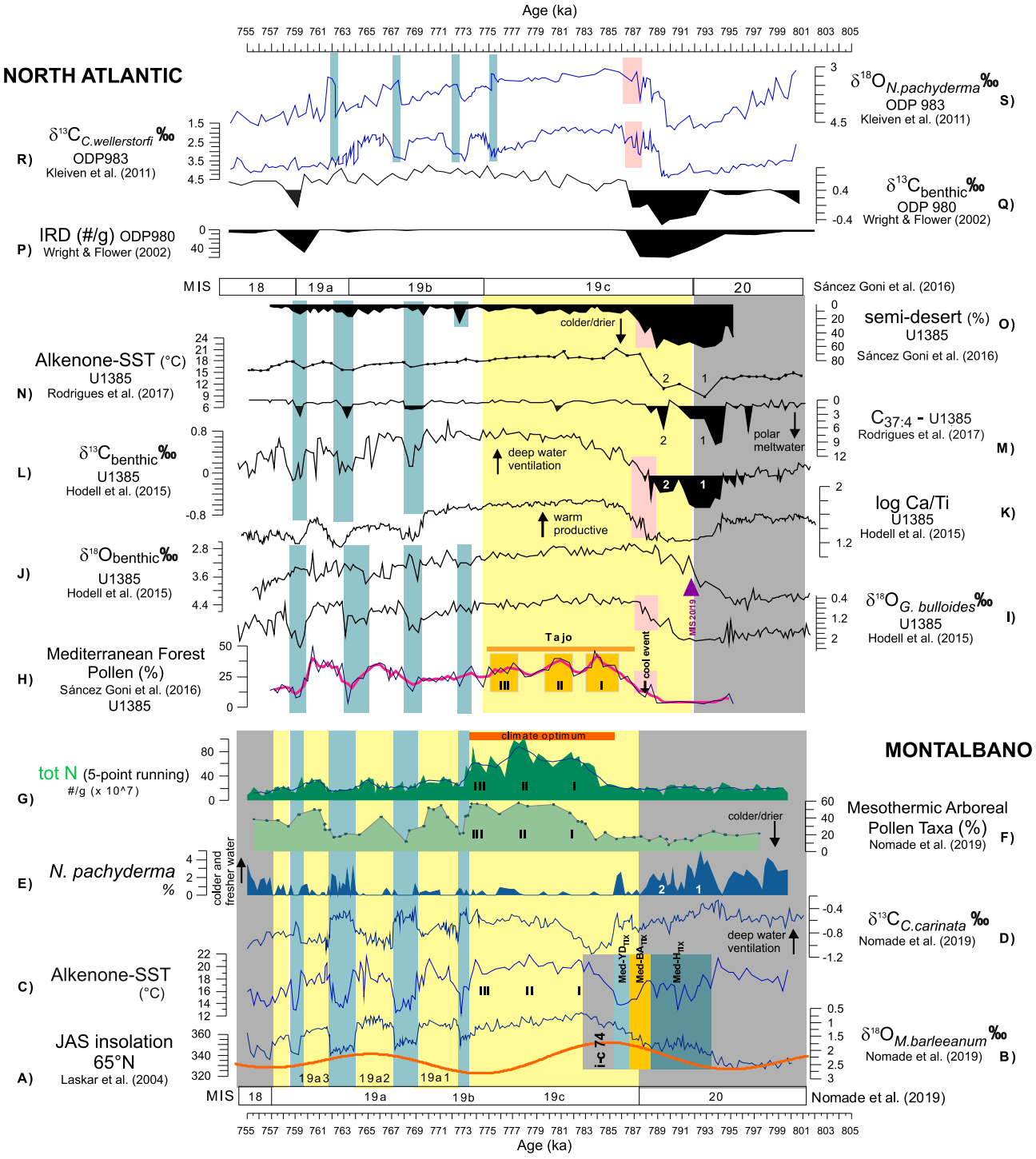

Fig. 4. Quantitative abundance patterns of *N. pachyderma* expressed as percentage (E) and of tot N (G, total abundance of coccoliths) expressed as number of coccoliths/g of sediment (#/g), pollen (F), alkenone-SST (C), benthic oxygen (B) and carbon (D) isotope records at the IS. Stage boundaries and climate optimum are marked according to Nomade et al. (2019) at the IS. A: mean summer insolation (JAS 65° N) from Laskar et al. (2004). Climate proxies from Iberian margin core U1385 (H-O), North Atlantic cores 980 (P-Q), 983 (R-S) are represented each in its original age model. Stage boundaries and Tajo phase are marked according to Hodell et al. (2015) and Sánchez Goñi et al. (2016) at the Iberian margin. Black arrow on Mediterranean Forest Pollen (H) marks the cool event according to Sánchez Goñi et al. (2016). Glacial MIS 20 and MIS 18 intervals are evidenced by grey bands. Light yellow color marks interglacial/interstadial phases. Light blue bands on proxy records are stadial phases. Green, dark yellow, blue and lilac bands on the isotope records at the IS represent Med-H_{TIX}, Med-BA_{TIX}, Med-YD_{TIX}, and ghost sapropel intervals, respectively. Pink bands on the North Atlantic record indicate intervals of climatic instability (see text). Numbers 1 and 2 on *N. pachyderma* curve at the IS indicate the two abundance peaks of the species in the Med-H_{TIX}, while they indicate nearly coeval, equivalent climate events on the U1385 records (see text). Numbers I-III are the main phases of ameliorated climate conditions in MIS 19c in the IS records and in the Mediterranean Forest Pollen at the U1385. (For interpretation of the references to colour in this figure legend, the reader is referred to the web version of this article.)

Mediterranean connection via atmospheric processes. Although the past atmosheric dynamic is poorly known, relatively more arid climate has been inferred at the IS during Ht in MIS 20 based on pollen assemblages (Bertini et al., 2015; Maiorano et al., 2016a). This is in agreement with the general arid conditions associated with recent Heinrich events (Allen et al., 1999; Combourieu Nebout et al., 2002; Sánchez Goñi et al., 2002; Naughton et al., 2016). Reduction of evaporation and precipitation has been also proven to occur even in the eastern Mediterranean during the Heinrich events (Bartov et al., 2003; Kwiecien et al., 2009).

Specifically, cold and dry Arctic air masses could have penetrated into the Ionian Sea during the winter season, similarly to what occurred during recent glacial cycles in the central and eastern Mediterranean region, and contributed, through enhanced north-westerly winds, to enhance winter deep water mixing and ventilation. The cold stadial phase during late MIS 20 in North Atlantic surface waters, as recorded by lower SST on the Iberian Margin (Fig. 4N), likely (i) reduced the evaporation and moisture content in air masses advected towards the Mediterranean region, promoting a cold and drier period, and (ii) induced more efficient north winter winds, and lower surface water temperature in the Ionian basin. This may have favored the proliferation of cold calcareous plankton taxa in sea surface water, as discussed above, and the arid conditions on land documented by pollen data at the IS (Bertini et al., 2015; Maiorano et al., 2016a). This seems in line with the higher aridity recorded at Site U1385 (Fig. 4O). Similar atmospheric mechanisms associated with oceanic circulation and linked to North Hemisphere ice-sheet dynamics have been suggested by Regattieri et al. (2019) and Nomade et al. (2019) to explain the high-frequency climate changes during MIS 19.

Therefore, we believe that the Atlantic colder climate phase in late MIS 20 may have affected the Ionian basin climate by both oceanographic connection through the Gibraltar Strait and polar air outbreaks over the Mediterranean (e.g. Allen et al., 1999; Cacho et al., 1999, 2006; Rohling et al., 2002; Frigola et al., 2008; Rodrigo-Gámiz et al., 2011; Sprovieri et al., 2012).

Sub-millennial scale variability and environmental instability are recorded by marine proxies within the Med-H_{TIX}, specifically in the oscillating SST values, with differences of temperatures up to 4 °C, and in the fluctuations of key calcareous plankton taxa (Fig. 2). In more detail, *N. pachyderma* shows two main abundance peaks (1 and 2 in Fig. 4E) that are surprisingly nearly coeval with two prominent lows in the $\delta^{13}C_{benthos}$ at the Site U1385 (low deep water ventilation, slowdown of AMOC) (1 and 2 in Fig. 4L). There, also SST and $C_{37:4}$ show a pattern with two phases of low and high values, respectively (colder and fresher/melting waters) (1 and 2 in Fig. 4 M-N). A two-fold pattern is additionally visible in the sea level curve (Fig. 2B) which shows two minima (although in a slightly different timing due to independent age models), that would be coherent with times of higher Atlantic meltwater and polar taxa influx. On the contrary, in the middle of Med-H_{TIX}, *G. inflata* (Fig. 2N) records fluctuating higher abundances, concurrent with fluctuating lower $\delta^{18}O$, indicating time of quite restored MAW inflow and periodic declines in the Atlantic meltwater arrival at the Mediterranean, possibly related to a short phase of less prominent low sea level (Fig. 2B). These data further sustain an Atlantic-Mediterranean hydrological connection even at shorter temporal scale. This variability, within the Med-H_{TIX}, is in line with abrupt changes recorded in Mediterranean Sea during climate phases correlated to Atlantic Heinrich events (Frigola et al., 2008; Martrat et al., 2014; Bazzicalupo et al., 2018). The centennial-scale variability seems to be a regular climate pattern of Heinrich events, when investigated at very high-resolution, as sustained by the moisture spells within the cold and arid H1 event on the northwestern Iberian margin (Naughton et al., 2011, 2016) and Iberian peninsula (Camuera et al., 2019), based on pollen signals. In the IS we cannot rule out that the multiple, sub-millennial scale changes may also be associated with discontinuous meltwater influence from mountain glaciers of southern Apennines through rivers or from Alpine chain through WAC. In fact, meltwater pulses from Italian peninsula chains have been documented during last termination and specifically from Alpine glaciers in the Adriatic Sea (Maselli et al., 2011).

6.2. Climate variability throughout Termination IX

Following the Med-H_{TIX}, the sea surface water interglacial warming, starting at about 785 ka, is preceded by an evident climate variability that is visible in the patterns of SST and selected calcareous plankton proxies (Fig. 2).

6.2.1. Med-BA_{TIX} and Med-YD_{TIX} events

The decrease of *C. pelagicus* ssp. *pelagicus* (Fig. 2L) and *N. pachyderma* (Fig. 2 K) and the remarkable peaks of *O. universa* (up to 25%) (Fig. 2O), together with the prominent increase of *Globorotalia inflata* (up to 80%) (Fig. 2N), represent the first signal of the climate amelioration during sea level rise, and may be associated with a Bølling-Allerød-like event (hereafter Med-BA_{TIX}). Decrease of Cupressaceae and increase of dinocysts *S. mirabilis/hyperacanthus*, the latter known to benefit from sea surface temperature between 10 and 15 °C during winter and between 15 and 22 °C during summer, confirm a climate amelioration (Maiorano et al., 2016a). This climate phase is now further supported by the alkenone-SST pattern, which records a distinct temperature increase of ca. 3 °C, up to 17.6 °C, from 788.4 to 786.1 ka, resembling the Bølling-Allerød-4 °C increase of the last termination in the western Mediterranean (Martrat et al., 2014). The SST profile during Med-BA_{TIX} marks a warming in the first phase followed by a cooling trend, and does not show distinct multiple oscillations like those occurred during the BA of last termination (North Greenland Ice Core Project members, 2004) that however recorded a similar general temperature decline. Nevertheless, within the Med-BA_{TIX}, the opposite pattern between *O. universa* and *G. inflata* could suggest that warm and fresh surface water conditions alternated in the region with period of normal salinity. *O. universa* in fact has a broad salinity tolerance and is most abundant in the vertically mixed layer and nutrient-rich areas of the low to mid-latitudes (Bé, 1977; Fairbanks et al., 1982; Pujol and Vergnaud-Grazzini, 1995; Morard et al., 2009). This taxon, during TI, calcified in low salinity waters derived by year-round return of meltwater before and after the main climate deterioration at the H1 and YD events (Spero and Williams, 1990; Vetter et al., 2017). Therefore, we infer that the occurrence of *O. universa* at the IS in the early and late portions of Med-BA_{TIX} may be evidence of short-term climate amelioration that destabilized and melted the local ice caps of the Apennines/Alpes areas leading to increased river runoff, which caused lower sea surface salinity, increase of detrital input and nutrient into the basin, preventing enhanced proliferation of warm and oligotrophic taxa (Fig. 2 G-H). Only the opportunistic species such as *O. universa* could have found suitable environmental conditions to proliferate. On the contrary, *G. inflata*, thriving under normal salinity conditions, records higher abundance in the mid Med-BA_{TIX}, since this species undergoes vertical migrations from shallow to intermediate water depths with low vertical salinity gradients (Martinez et al., 2007) and deep pycnocline, in relation to recovered Atlantic-Mediterranean water exchange and sea level rising (Fig. 2B), similarly to what occurred during Bølling-Allerød (Sprovieri et al., 2003; Lirer et al., 2013).

Upwards, the following and gradual SST decrease of ca 2.5 °C centered at 785.8 ka, together with short-term increases of the polar-subpolar *N. pachyderma, C. pelagicus* ssp. *pelagicus,* and of *N. incompta* (Fig. 2), sustain a very short-term cool spell, before interglacial warming inception, that is interpreted as a Younger Dryas-like event (hereafter Med-YD_{TIX}). A slight but distinct increase of benthic $\delta^{13}C$ (Fig. 2P) during the Med-YD_{TIX} marks a short-term restored sea bottom ventilation and deepening of mixed layer. Such environmental conditions may have been driven by more efficient winter winds during an arid period, in agreement with the decreased precipitation/rainfall recorded in the central Italy during the coeval "YD" at TIX (Giaccio et al.,

2015). Similar sequence of warm and cold short term episodes just before the MIS 19c onset has been recognized in the Ionian Sea (core KC01B) based on the pattern of coccolithophore taxa (Trotta et al., 2019), and Balearic basin based on calcareous plankton assemblages and alkenone-SST (Quivelli, 2020), thus attesting high-frequency climate changes through TIX at the scale of Mediterranean basin.

The millennial climate variability across the MIS 20-MIS 19 deglaciation, that can be reconstructed in the IS, improves our understanding of climate evolution during terminations. Such high-frequency changes seem to be a shared feature of most terminations over the last 800 ka (Barker et al., 2019), especially during times of intermediate glacial ice volume, as it is the case of MIS 20, and transitions between glacial and interglacial state (Ruddiman et al., 2016).

6.2.2. Comparison of TIX between Ionian and Atlantic records

On the whole, the new data-set that we obtained through TIX (Med-BA_{TIX} and Med-YD_{TIX}) at the IS reinforces the working hypothesis that there should be a strong similarity between TIX and TI recorded in the Mediterranean Sea (Capotondi et al., 1999; Sbaffi et al., 2001; Asioli et al., 2001; Di Stefano and Incarbona, 2004; Siani et al., 2010, 2013; Geraga et al., 2010; Rouis-Zargouni et al., 2010; Castañeda et al., 2010; Kontiokis, 2016; Bazzicalupo et al., 2018).

Although analogy with Bølling-Allerød-type and Younger-Dryas-type episodes has not been inferred so far in oceanic waters out of the Mediterranean during TIX, we compared our results to selected high-resolution North Atlantic sedimentary records (Fig. 4). They evidence instability in surface and subsurface waters and in climate on land during the MIS 20–19 transition (Fig. 4 H-I, K-L, O, R-S, pink bands). Even though a correlation between Med-BA_{TIX} and Med-YD_{TIX} events at the IS and specific fluctuations in the North and northern Atlantic climate records (Fig. 4) may not be unambiguous, we would stress that evident oscillations may be observed at the core U1385 in the final decreasing trend of semi-desert and Mediterranean Forest Pollen curves (pink bands, Fig. 4H, O), before the beginning of Tajo phase. The cool spell event (black arrow in Fig. 4H) just above a short-term slight increase in Mediterranean Forest Pollen resembles the cool Med-YD_{TIX} following the Med-BA_{TIX} and just before the climate optimum at the IS. Besides, the $\delta^{13}C_{benthos}$ and log Ca/Ti curves (Fig. 4J-K) indicate short-term climate variations at the Iberian margin in terms of Atlantic Ocean deep-water ventilation/stratification, temperature, and marine productivity, respectively. Similar fluctuations are shown by the $\delta^{18}O_{plankton}$ and $\delta^{13}C_{benthos}$ at the northern Atlantic Site 983 (pink band in Fig. 4 R-S), once more suggesting short-lived changes in temperature, salinity and deep-water ventilation, and in AMOC strength. This unstable phase has been interpreted as a result of no full recovery of ocean circulation (AMOC interglacial mode) and decrease of atmospheric CO_2 (Ruddiman et al., 2016; Barker et al., 2019). Therefore, a link between North Atlantic (AMOC instability) and central Mediterranean climate during deglaciation MIS 20-MIS 19 may be inferred. However, a full rigorous discussion on the relationships between the different climate proxies or on the timing and propagation of climate signals during TIX among the different areas needs additional investigations.

6.3. The Ionian Sea "ghost sapropel"-insolation cycle 74

Following the Med-YD_{TIX} event, in the lowermost climate optimum of MIS 19c (Fig. 3), the SST record reveals a quite sharp increase up to 16.5 °C at 785 ka together with higher foram-wwt (Fig. 2H), very close to the mean summer insolation maximum (785.4 ka) (Fig. 3I). While, total N (Fig. 3C) and nanno-wwt (Fig. 3D) do increase just above, suggesting that favorable, stable conditions for the calcareous phytoplankton did occur not before 784 ka, when temperatures were higher than 18.5 °C (Fig. 3B). The correlation index (R) between total N and alkenone-SST and between nanno-wwt and alkenone-SST are quite positive, respectively +0.50 and + 0.69, and this may suggest that not only temperature but also specific trophic conditions may have influenced coccolithophore productivity. With respect to Maiorano et al. (2016a) and Nomade et al. (2019), here, some additional elements may help in revealing variable environments during the ghost sapropel deposition (lilac band in Fig. 3). During the lower $\delta^{13}C_{C.carinata}$ values, a general high *G. ruber* abundance is recorded (Fig. 3D), indicative of warm oligotrophic and stratified surface waters (Bé and Hamlin, 1967; Bé, 1971; Bé and Tolderlund, 1971; Hemleben et al., 1989; Pujol and Vergnaud-Grazzini, 1995). However, the taxon shows a distinct decrease at 783.5 ka, at the $\delta^{13}C_{C.carinata}$ minimum (Fig. 3J), whereas *F. profunda* and *Syracosphaera* spp. (Fig. 3F-G) show a peak. *Syracosphaera* spp. are capable to tolerate less saline and turbid surface water (Weaver and Pujol, 1988; Colmenero-Hidalgo et al., 2004; Maiorano et al., 2013, 2016a, 2016b), and *F. profunda* may thrive in low light surface waters when high turbidity and nutrient availability drive the taxon upwards (Ahagon et al., 1993; Colmenero-Hidalgo et al., 2004; Maiorano et al., 2008, 2016a; Girone et al., 2013). These combined patterns at 783.5 ka suggest enhanced runoff/organic matter input from surrounding hinterland, close to insolation maximum and North Africa monsoon strengthening, promoting enhanced low oxygen conditions and organic matter preservation at the sea floor. *G. bulloides* (Fig. 3H), that records a contemporary prominent abundance peak at 783.5 ka and an opposite pattern with respect to $\delta^{13}C_{C.carinata}$ during sapropel deposition, may have been favored in such conditions as it is an opportunistic species that proliferates in eutrophic environments. Accordingly, low total coccolithophore abundance (Fig. 3C) is likely related to turbidity increase by river terrigenous input in the Montalbano Jonico basin also supported by coarser sediment at this time (Maiorano et al., 2016a). The enhanced detrital input is a common signature observed during sapropel layers in the MJS as recorded in the older sapropels i-cycles 112, 102, and i-c 86 in the lower portion of the section (Fig. 1C) (Maiorano et al., 2008; Girone et al., 2013). Starting from the $\delta^{13}C_{C.carinata}$ minimum and the decreasing trend of *G. bulloides* (Fig. 3H), more stable and oligotrophic surface water conditions restored with respect to the first sapropel phase. A very short-term peak of *Braarudosphaera bigelowii* (Fig. 3E), although with low abundances, marks a low salinity spell at the end of sapropel, concurrent with increasing trend of $\delta^{13}C$ (Fig. 3J), in agreement with data of Narciso et al. (2010) for the end of sapropel S5 during MIS 5.5 in the Adriatic Sea.

It is worth to note that the organic rich layer (ORL) i-cycle 74 recognized in the Balearic Sea at the TIX (Quivelli et al., 2020) supports the basin-scale character of this oceanographic event and the occurrence of ORL in the western Mediterranean slightly before the sapropel deposition in eastern basin (Rogerson et al., 2008).

6.4. Was MIS 19c a stable full interglacial?

During MIS 19c, higher SST and calcareous plankton warm water taxa, and enhanced values of total coccolith production (> 60 and up to 100 coccoliths/g x 10^7) (Fig. 2D, F-H), starting from the post sapropelic layer, are the response to climate amelioration. SST values, mainly between 18 and 21.9 °C (Fig. 2D), are very similar to modern ones, and are similar to Holocene values in the region (Alkenone-SST, Emeis et al., 2000b) and in the western Mediterranean (Alkenone-SST, Cacho et al., 2001; Martrat et al., 2014). A higher temperature value (25 °C) has been provided by Peral et al. (2020) at the IS based on *G. ruber*-Mg/Ca estimate in one sample from MIS 19, at the level just above the end of sapropel (~781.5 ka). Nevertheless, the authors discuss possible biases of the Mg/Ca method in the Mediterranean Sea.

Two subtle phases may be distinguished at the IS during MIS 19c based on planktonic foraminifera. The first phase, starting about 2 kyr after the end of sapropel up to 780 ka, was characterized by seasonal contrast with slightly lower winter temperatures, which were able to induce mixing and advection of nutrients to the surface waters, and the development of seasonal Deep Chlorophyll Maximum (DCM) over warm, well stratified and oligotrophic waters in summer. This inference is based on the occurrence of *N. incompta* (Fig. 2I), and, although with

very low abundances, of *G. inflata* (Fig. 2N). Similar conditions immediately after the end of S1 have been documented in all records from eastern Mediterranean, Adriatic and Ionian basins during the Holocene (Rohling et al., 1997; Capotondi et al., 1999; De Rijk et al., 1999; Geraga et al., 2000, 2008). The second phase of MIS 19c at the IS, from about 780 ka to the end of full interglacial, is characterized by the absence of *N. incompta* and *G. inflata* in relation to higher abundances of *G. ruber* (Fig. 3D), suggesting that during the late MIS 19c the prevailing environmental conditions in the Ionian basin were closer to those of the modern Levantine basin than to the modern western Mediterranean Sea. Such a frame may be associated with a more permanent cyclonic regime in the Ionian Sea (Fig. 1D) leading the northern internal border of the basin under the direct influence of poor-nutrient LIW (Civitarese et al., 2010). This is consistent with the modern regional distribution of *G. inflata* that it is absent in the northern Ionian Sea (Mallo et al., 2017; Di Donato et al., 2019) but occurs in the southern basin following the path of Atlantic waters that, under cyclonic regime, does not arrive in the northern sector of the basin. There, during the last 6 kyr, starting from about 2 kyr after the end of the Holocene S1 deposition (like at the IS after ghost sapropel i-cycle 74), *G. inflata* is absent, with the exception of short incursions during period of reversed circulation (Fig. 1E) (Di Donato et al., 2019).

Higher frequency changes in the environmental conditions may be distinguished during MIS 19c. Specifically, several oscillations in about 11 kyr may be observed in total N and SST curves (Fig. 2D, F). These fluctuations are fairly in-phase; however, if smoothed-out by a 5-point running average, they more clearly appear as three main warmer phases (purple arrows in Fig. 2D, F-G). The curve of Mesothermic arboreal pollen (MAP) taxa at the IS (Fig. 2E), although at low resolution, seems to record a similar pattern as well, pointing to an in-phase high climate variability in both marine and continental settings, and then implying both oceanographic and atmospheric processes. The main increases of MAP taxa at the IS may be linked to southward westerly shift and higher winter precipitation in south Europe and Mediterranean basin (Wagner et al., 2019), perhaps in analogy to processes operating like the modern or recent North Atlantic Oscillation mode (Xoplaki et al., 2003; Moreno et al., 2002, 2004, 2005; Hurrell et al., 2004; Roberts et al., 2008; Fletcher et al., 2009; Ulbrich et al., 2012). The main increases of nanno-wwt in sea surface water (Fig. 2G) would be the result of increased inflow of warm tropical-subtropical waters through the Gibraltar Strait toward central Mediterranean.

Additional seasonal climate insights derive from the distribution pattern of foraminifer *Trilobatus sacculifer* (Fig. 2 H), a tropical-subtropical taxon (Bé, 1977; Vincent and Berger, 1981) that has a peculiar occurrence in MIS 19c, showing multiple oscillations and an opposite distribution with respect to *G. ruber*. The higher abundance of *T. sacculifer* could be related to low seasonality and milder winters (Bé and Hutson, 1977; Vincent and Berger, 1981; Hemleben et al., 1989; Fraile et al., 2008), or to short term periods of relative less humid conditions. This is in accordance with findings during MIS 19 in the Alboran Sea (Toti et al., 2020), during MIS 11 (Maiorano et al., 2016b; Marino et al., 2018) and Holocene in the Mediterranean and Red Sea basins (Piva et al., 2008; Edelman-Furstenberg et al., 2009). A slight reduction of MAP taxa in the upper MIS 19c during higher abundance of *T. sacculifer* (Fig. 2) could sustain this interpretation.

The unstable climate character of MIS 19c has been recorded in the high-resolution records from central Italy Sulmona (Regattieri et al., 2019) and U1385 sediments (Sánchez Goñi et al., 2016). In particular, three main increases of the Mediterranean Forest Pollen during Tajo phase were detected on the Iberian margin similarly to what occurs in the MIS 19c at the IS. While, a decoupled response between terrestrial (pollen, Fig. 4 H, O) and marine ($C_{37:4}$, alkenone-SST, Fig. 4 M-N) signals (the latter recording a certain stability throughout the entire full interglacial) was evidenced at Site U1385. This was explained as a direct and synchronous response of Iberian vegetation to northern Atlantic climate via atmospheric process (like at the IS), whereas sea surface temperatures remained almost stable at the location of Site U1385 due to the effect of warm retaining of subtropical gyre (Repschläger et al., 2015). It is possible that during MIS 19c the common feature of vegetation patterns, as recorded in IS and Iberian margin, was a shared response to atmospheric processes that in concert also influenced the marine proxies (mainly total N and coccolithophore wwt) in the Ionian Sea, contrary to what happened in the Atlantic waters west of Iberia.

6.5. The stadial-interstadial phases in MIS 19b-a

The first signal of climate deterioration at the end of full interglacial MIS 19c occurs at ~773–774 ka when alkenone-SST displays a prominent drop of about 8-9 °C with a minimum of 12.1 °C at 772.8 ka (Fig. 2D); this temperature drop is even stronger than in Med-H_{TIX}. Warm water taxa decrease at the same time (Fig. 2 G-H), thus marking the first significant cooling and the substage MIS 19b (Figs. 2, 4). MIS 19b is very distinctive in the IS, being very close to the Ar/Ar dated V4 and $^{10}Be/^{9}Be$ peak (interpreted as the Earth magnetic field collapse during the Matuyama-Brunhes reversal, Simon et al., 2017), and associated with the beginning of polar ice-sheet increase and instability (Maiorano et al., 2016a), synchronously with the first IRD occurrence after full interglacial MIS 19 in northern Atlantic (Kleiven et al., 2011). At this time, the MAP taxa (Fig. 2E) decrease while the steppic and halophyte vegetation advances at the IS, highlighting cold and arid conditions over the central Mediterranean hinterland (Bertini et al., 2015). A quite concurrent slight increase of semi-desert vegetation centered at ~772.6 ka (Fig. 4O) and decrease of Mediterranean Forest Pollen (Fig. 4H) occur at the core U1385, suggestive of a cooling/arid episode on the southwestern Iberian. On the other hand, no coeval variation occurs in the alkenone records at the Site U1385 (Fig. 4M-N). Our data-set at the IS seems to underline that at the time of MIS 19b the response of calcareous plankton (Fig. 2F-G, L) and alkenone-SST (Fig. 2 D) is clearly in phase with the vegetation response (Fig. 2 E), and both are in phase with the pollen data at the Iberian margin (Fig. 4M, O). While at Site U1385 the subtropical gyre was responsible for the presence of still warm waters, which likely reduced the arrival of polar-subpolar taxa at the Ionian basin (Fig. 2 K-L), a southward influx of cold and dry arctic air masses towards the IS location promoted efficient cooling of SST and terrestrial environments, maybe more efficiently than during Med-H_{TIX}. It is possible that continental cold and dry air flux by enhanced Siberia High pressure had a role in the central Mediterranean at this time. An equivalent pattern is seen in the Holocene record in the eastern Mediterranean, where intensified Siberia High has been suggested for the cold and dry spell at 8.2 ka (Pros et al., 2009).

Above MIS 19b, the most prominent feature of climate evolution in the IS is the occurrence of multiple oscillations in all climate proxies (Figs. 2, 4) that are related to the reestablishment of millennial-scale variability and, presumably, of the bipolar seesaw (Tzedakis et al., 2012). This climate trend toward the glacial stage 18 onset is very well recorded at the IS, as widely discussed in Nomade et al. (2019, to whom we refer) based on oxygen and carbon isotopes, and is now finely improved by our new data-set (Fig. 2). The three distinct warm oscillations during MIS 19a (19a-1, 19a-2, and 19a-3) at the IS are evidenced by the impressive parallel fluctuating increase/decrease of alkenone-SST pattern as well as of warm and cold water taxa indicators (Figs. 2-4). In addition, total coccolith production increased during warmer interstadial phases; these were characterized by lower deepwater ventilation (lower $\delta^{13}C$, Fig. 2P), even if not as pronounced as during sapropel deposition in MIS 19c (Fig. 2). The inceptions of these interstadials were characterized not only by sudden warming but also by abrupt changes in the surface hydrological regime in the basin. This paleoenvironmental reconstruction is based on the sharp increases of *O. universa* at the beginning of the interstadials 19a-1 and 19a-2, when the SST did not reach maximum values, the $\delta^{13}C$ was lower than in the second half of interstadials, and the stadial-interstadial $\delta^{18}O$ lightening

shifts are very sharp. We believe that abrupt climate amelioration at the onset of interstadials would have destabilized local mountain glaciers resulting in the return of local meltwater input into the basin. This frame reflects superimposed local process on global climate signals and definitively sustains the local freshwater discharge hypothesized by Nomade et al. (2019) to explain the very rapid (< 200 years) and high-amplitude stadial-interstadials oscillations described by the $\delta^{18}O$ record during MIS 19a. Wetter climate conditions on land, as suggested by pollen assemblages at the IS (Fig. 2E), contributed to increase the freshening conditions of sea surface waters leading to the reduction of bottom water ventilation (low benthic $\delta^{13}C$), in agreement with the higher precipitation over the Italian peninsula documented by both the Pianico-Sellere and Sulmona paleolake records (Moscariello et al., 2000; Rossi, 2003; Giaccio et al., 2015; Nomade et al., 2019). Such a pattern points to a marked correspondence between terrestrial and marine records and then between atmospheric and oceanographic processes during MIS 19a in the central Mediterranean. Among the interstadials, 19a-2 appears as the warmest, in agreement with higher SST and the occurrence of tropical *T. sacculifer* (Fig. 2 H), suggesting the establishment of surface water condition similar to the MIS 19c climate optimum. In the final part of MIS 19a, the shallowing trend of the Montalbano basin has been reconstructed (Ciaranfi et al., 2010, and references therein), simultaneous with a global sea level lowering trend (Fig. 2B). The lower depths during stadials of MIS 19a were characterized by increased turbidity in surface water, as evidenced by higher *H. carteri* abundances (Fig. 2M) that, like during glacial MIS 20, increase in relation to times of lower sea level, which enhances erosion on land and inorganic input influx into the basin. A cooling trend toward the top of the study section up to the MIS 18 glacial onset at 757 ka (Nomade et al., 2019) co-occurs, and is sustained by the heavier values of $\delta^{18}O$ together with the increased occurrence of cold water taxa *C. pelagicus* ssp. *pelagicus* and *N. pachyderma* and decreasing trend of wwt and total N (Fig. 2).

7. Conclusions

The high-resolution data-set obtained at the IS based on alkenone-SST and calcareous plankton analyses, combined with the available high-resolution $\delta^{18}O$ and $\delta^{13}C$ records, evidence orbital-suborbital climate oscillations, which delineate a detailed climatostratigraphic frame through late MIS 20 to early MIS 18. This is a crucial time interval of the mid-Pleistocene transition that includes the Lower-Middle Pleistocene chronostratgraphic boundary close to the Matuyama-Brunhes paleomagnetic reversal associated with MIS 19c/MIS 19b.

The alkenone-SST, representing the first record in the Mediterranean Sea in this time interval, distinctly records the climate pattern across MIS 20–18 and makes it possible to identify substages and shorter-term climate variations. The oscillations of SST and calcareous plankton key taxa confirm that there exists a strong analogy between TIX and last deglaciation, and sustain the identification of Heinrich-type, BA-type and YD-type events during TIX, here named Med-H_{TIX}, Med-$BA_{TIX,}$ and Med-YD_{TIX}, respectively. The recognition of these episodes improves our knowledge on the climate evolution during terminations of last 800 kyr. Multiple very short-term SST fluctuations characterized the Med-H_{TIX} event confirming the regular, unstable climate pattern of Heinrich events when studied at very high-resolution. The Med-BA_{TIX} is marked by higher SST at the beginning followed by a long cooling trend towards the Med-YD_{TIX} episode. The paleoenvironmental conditions during the ghost sapropel occurring at the beginning of interglacial 19, during insolation maximum (i-cycle 74), are characterized by sub-millennial scale internal variability, and synchronously displayed by the multiple proxies.

Unstable conditions in MIS 19c have been discovered, with three main phases of increased SST, calcareous plankton warm water taxa, and total coccolithophore production. Higher frequency variability has been revealed by the uppermost surface water proxies and corresponds to multiple pulses of tropical-subtropical water inflow into the basin. The distinct climate fluctuations in MIS 19b-a interval are the result of global climate changes being correlatable worldwide, but they are emphasized by the location of the IS close to Italian hinterland, suited to record local changes in freshwater/detrital/nutrient inputs, influencing the calcareous plankton taxa, and reveailing them as powerful proxies for detailing environmental reconstruction.

Comparison of our results with selected mid- and high-latitude North Atlantic marine and terrestrial climate proxies, pinpoints the occurrence of similar climate oscillations, in spite of the different age models among sites and the influence of different control factors in diverse oceanographic settings. Data suggest that the North Atlantic and polar climate dynamics strongly affected the climate evolution at the IS location and that atmospheric processes, other than oceanographic, may have had a prominent role in marine and terrestrial environments in central Mediterranean. The clarification of timing and areal propagation of climate signals through oceanographic and/or atmospheric connection requires, however, additional high-resolution multi-proxy studies from different regions in well-constrained chronological frameworks.

Declaration of Competing Interest

None.

Acknowledgments

This research was financially supported by Università degli Studi di Bari Aldo Moro, Fondi di Ateneo P. Maiorano, 2016 and benefited of instrumental upgrades from “Potenziamento Strutturale PONa3_00369 dell'Università degli Studi di Bari, Laboratorio per lo Sviluppo Integrato delle Scienze e delle TEcnologie dei Materiali Avanzati e per dispositivi innovativi (SISTEMA)”. The authors thank the editor and two anonymous referees, which improved the first version of the manuscript. M.M. is grateful to M.F. Sáncez Goñi for providing vegetation data-set at core U1385.

Declaration of Competing Interest

None.

References

Ahagon, N., Tanaka, Y., Ujiie, H., 1993. Florisphaera profunda, a possible nannoplankton indicator of late Quaternary changes in sea-water turbidity at the northwestern margin of the Pacific. Mar. Micropaleontol. 22, 255–273.

Aiello, G., Barra, D., Parisi, R., 2015. Lower-Middle Pleistocene ostracod assemblages from the Montalbano Jonico section (Basilicata, southern Italy). Quat. Int. 383, 47–73. https://doi.org/10.1016/j.quaint.2014.11.010.

Allen, J.R., Brandt, U., Brauer, A., Hubberten, H.W., Huntley, B., Keller, J., Nowaczyk, N.R., 1999. Rapid environmental changes in southern Europe during the last glacial period. Nature 400 (6746), 740.

Amore, F.O., Flores, J.A., Voelker, A.H.L., Lebreiro, S.M., Palumbo, E., Sierro, F.J., 2012. A Middle Pleistocene Northeast Atlantic coccolithophore record: paleoclimatology and paleoproductivity aspects. Mar. Micropaleontol. 90-91, 44–59.

André, A., Weiner, A., Quillévéré, F., Aurahs, R., Morard, R., Douady, C.J., de Garidel-Thoron, T., Escarguel, G., de Vargas, C., Kucera, M., 2013. The cryptic and the apparent reversed: lack of genetic differentiation within the morphologically diverse plexus of the planktonic foraminifer Globigerinoides sacculifer. Paleobiology 39 (1), 21–39.

Asioli, A., Trincardi, F., Lowe, J.J., Ariztegui, D., Langone, L., Oldfield, F., 2001. Submillennial-scale climatic oscillations in the central Adriatic during the Late glacial: palaeoceanographic implications. Quat. Sci. Rev. 20, 1201–1221.

Aurahs, R., Treis, Y., Darling, K., Kucera, M., 2011. A revised taxonomic and phylogenetic concept for the planktonic foraminifer species Globigerinoides ruber based on molecular and morphometric evidence. Mar. Micropaleontol. 79, 1–14.

Azzaroli, A., Perno, U., Radina, B., 1968. Note illustrative della Carta Geologica d'Italia alla scala 1:100.000, Foglio 188 Gravina di Puglia: Servizio Geologico Italiano. (57 pp).

Bárcena, M.A., Flores, J.A., Sierro, F.J., Pérez-Folgado, M., Fabres, J., Calafat, A., Canals, M., 2004. Planktonic response to main oceanographic changes in the Alboran Sea (Western Mediterranean) as documented in sediment traps and surface sediments.

Mar. Micropaleontol. 53 (3–4), 423–445.
Barker, S., Knorr, G., Conn, S., Lordsmith, S., Newman, D., Thornalley, D., 2019. Early interglacial legacy of deglacial climate instability. Paleoceanogr. Paleoclimatol. https://doi.org/10.1029/2019PA003661.
Bartov, Y., Goldstein, S.L., Stein, M., Enzel, Y., 2003. Catastrophic arid episodes in the eastern Mediterranean linked with the North Atlantic Heinrich events. Geology 31, 439–442.
Bassinot, F., Labeyrie, L., Vincent, E., Quidelleur, X., Shackleton, N., Lancelot, Y., 1994. The astronomical theory of climate and the age of the Brunhes-Matuyama magnetic reversal. Earth Planet. Sci. Lett. 126 (1–3), 91–108. https://doi.org/10.1016/012-821X(94)90244-5.
Batistić, M., Viličić, D., Kovačević, V., Jasprica, N., Lavignec, H., Carića, M., Garić, R., Cara, A., 2017. Winter phytoplankton blooms in the offshore south Adriatic waters (1995-2012) regulated by hydroclimatic events: Special emphasis on the exceptional bloom of 1995. Biogeosci. Discuss. https://doi.org/10.5194/bg-2017-205.
Baumann, K.-H., Andruleit, H., Samtleben, C., 2000. Coccolithophores in the Nordic Seas: comparison of living communities with surface sediment assemblages. Deep-Sea Res. II Top. Stud. Oceanogr. 47, 1743–1772.
Baumann, K.-H., Bockel, B., Frenz, M., 2004. Coccolith contribution to South Atlantic carbonate sedimentation. In: Thierstein, H.R., Young, J. (Eds.), Coccolithophores: From Molecular Processes to Global Impact. Springer, Berlin, pp. 367–402.
Bazzicalupo, P., Maiorano, P., Girone, A., Marino, M., Combourieu-Nebout, N., Incarbona, A., 2018. High-frequency climate fluctuations over the last deglaciation in the Alboran Sea, Western Mediterranean Sea: evidence from calcareous plankton assemblages. Palaeogeogr. Palaeoclimatol. Palaeoecol. 506, 226–241.
Bé, A.W.H., 1971. Winter distribution of planktonic foraminifera between the Grand Banks and the Caribbean. Micropalaeontology 17 (1), 31–42.
Bé, A.W.H., 1977. An ecological, zoogeographic and taxonomic re view of recent planktonic foraminifera. In: Ramsay, A.T.S. (Ed.), Oceanic Micropaleontology. vol. 1. Academic Press, London, pp. 1.
Bé, A.W.H., Hamlin, W.H., 1967. Ecology of recent planktonic foraminifera. Micropaleontology 13, 87–100.
Bé, A.W.H., Hutson, W.H., 1977. Ecology of Planktonic Foraminifera and Biogeographic Patterns of Life and Fossil Assemblages in the Indian Ocean. Micropaleontology. vol. 23(4). The Micropaleontology Project., Inc, pp. 369. https://doi.org/10.2307/1485406.
Bé, A.W.H., Tolderlund, D.S., 1971. Distribution and ecology of living planktonic foraminifera in surface waters of the Atlantic and Indian Oceans. In: Funnell, B.M., Riedel, W.R. (Eds.), The Micropaleontology of the Oceans, pp. 105–149.
Bélthoux, G.P., 1979. Budgets of the Mediterranean Sea: their dependence on the local climate and on the characteristics of the Atlantic waters. Ocean. Acta 2, 157–163.
Bertini, A., Toti, F., Marino, M., Ciaranfi, N., 2015. Vegetation and climate across the Early-Middle Pleistocene transition at the Montalbano Jonico section (southern Italy). Quat. Int. 383, 74–88. https://doi.org/10.1016/j.quaint.2015.01.003.
Bignami, F., Sciarra, R., Carniel, S., Santoleri, R., 2007. Variability of Adriatic Sea coastal turbid waters from SeaWiFS imagery. J. Geophys. Res. 112, C03S10. https://doi.org/10.1029/2006JC003518.
Boeckel, B., Baumann, K.-H., 2004. Distribution of coccoliths in surface sediments of the south-eastern South Atlantic Ocean: ecology, preservation and carbonate contribution. Mar. Micropaleontol. 51 (3–4), 301–320.
Boenzi, F., Capolongo, D., Gallicchio, S., Di Pinto, G., 2014. Morphostructure of the Lucania Apennines front between the Basento and Salandrella rivers (Southern Italy). J. Maps 10 (3), 478–486.
Bonomo, S., Cascella, A., Alberico, I., Lirer, F., Vallefuoco, M., Marsella, E., Ferraro, L., 2018. Mar. Micropaleontol. 142, 67–91. https://doi.org/10.1016/j.marmicro.2018.06.003.
Brückner, H., 1980a. Marine Terrassen in Süditalien. Eine quartärmorphologische Studie über das Küstentiefland von Metapont. Düsseldorfer Geographische Schriften 14 (235 pp).
Brückner, H., 1980b. Flußterrassen und flußtäler im Küstentiefland von Metapont (Süditalien) und ihre Beziehung zu Meeresterrassen. Düsserdolfer G eographische Schriften 15, 5–32.
Cacho, I., Grimalt, J.O., Pelejero, C., Canals, M., Sierro, F.J., Flores, J.A., Shackleton, N.J., 1999. Dansgaard-Oeschger and Heinrich event imprints in the Alboran Sea paleotemperatures. Paleoceanography 14, 698–705.
Cacho, I., Grimalt, J.O., Sierro, F.J., Shackleton, N.J., Canals, M., 2000. Evidence for enhanced Mediterranean thermohaline circulation during rapid climatic coolings. Earth Planet. Sci. Lett. 183, 417–429.
Cacho, I., Grimalt, J.O., Canals, Sbaffi, M. L., Shackleton, J., Schonfeld, J., Zahn, R., 2001. Variability of the western Mediterranean Sea surface temperature during the last 25, 000 years and its connection with the Northern Hemisphere climatic change. Paleoceanography 16(1), 40–52. DOI: https://doi.org/10.1029/SP010.
Cacho, I., Shackleton, N., Elderfield, H., Sierro, F.J., Grimalt, J.O., 2006. Glacial rapid variability in deep-water temperature and $\delta^{18}O$ from the Western Mediterranean Sea. Quat. Sci. Rev. 25, 3294–3311.
Camuera, J., Jiménez-Moreno, G., Ramos-Román, M.J., García-Alix, A., Jiménez-Espejo, F., Toney, J.L., Anderson, R.S., Webster, C., 2019. Climatic subdivision of Heinrich Stadial 1 based on centennial-scale paleoenvironmental changes observed in the western Mediterranean area. Clim. Past Discuss. https://doi.org/10.5194/cp-2019-130.
Capotondi, L., Borsetti, A.M., Morigi, C., 1999. Foraminiferal ecozones, a high-resolution proxy for the late Quaternary biochronology in the central Mediterranean Sea. Mar. Geol. 153, 253–274.
Capotondi, L., Girone, A., Lirer, F., Bergami, C., Verducci, M., Vallefuoco, M., Afferri, A., Ferraro, L., Pelosi, N., De Lange, G.J., 2016. Central Mediterranean Mid-Pleistocene paleoclimatic variability and its connection with global climate. Palaeogeogr. Palaeoclimatol. Palaeoecol. 442, 72–83.
Casford, J.S.L., Rohling, E.J., Abu-Zied, R.H., Fontanier, C.F., Jorissen, J., Leng, M.J., Schmiedl, G., Thomson, J., 2003. A dynamic concept for eastern Mediterranean circulation and oxygenation during sapropel formation. Palaeogeogr. Palaeoclimatol. Palaeoecol. 190, 103–119.
Casnedi, R., 1988. La Fossa bradanica: origine, sedimentazione e migrazione. Mem. Soc. Geol. Ital. 41, 439–448.
Castañeda, I.S., Schefuß, E., Pätzold, J., Sinninghe Damsté, J.S., Weldeab, S., Schouten, S., 2010. Millennial-scale sea surface temperature changes in the eastern Mediterranean (Nile River Delta region) over the last 27,000 years. Paleoceanography 25 (1).
Ciaranfi, N., D'Alessandro, A., 2005. Overview of the Montalbano Jonico area and section: a proposal for a boundary stratotype for the lower-middle Pleistocene, southern Italy Foredeep. Quat. Int. 131, 5–10.
Ciaranfi, N., Lirer, F., Lirer, L., Lourens, L.J., Maiorano, P., Marino, M., Petrosino, P., Sprovieri, M., Stefanelli, S., Brilli, M., Girone, A., Joannin, S., Pelosi, N., Vallefuoco, M., 2010. Integrated stratigraphy and astronomical tuning of the Lower-Middle Pleistocene Montalbano Jonico land section (southern Italy). Quat. Int. 210, 109–120.
Civitarese, G., Gačič, M., Lipizer, M., Eusebi Borzelli, G.L., 2010. On the impact of the Bimodal Oscillating System (BiOS) on the biogeochemistry and biology of the Adriatic and Ionian Seas (Eastern Mediterranean). Biogeosciences 7, 3987–3997. https://doi.org/10.5194/bg-7-3987-2010.
Colmenero-Hidalgo, E., Flores, J.A., Sierro, F.J., Barcena, M.A., Lowemark, L., Schonfeld, J., Grimalt, J.O., 2004. Ocean surface water response to short-term climate changes revealed by coccolithophores from the Gulf of Cadiz (NE Atlantic) and Alboran Sea (W Mediterranean). Palaeogeogr. Palaeoclimatol. Palaeoecol. 205, 317–336.
Combourieu Nebout, N., Turon, J.L., Zahn, R., Capotondi, L., Londeix, L., Pahnke, K., 2002. Enhanced aridity and atmospheric high-pressure stability over the western Mediterranean during the North Atlantic cold events of the past 50 ky. Geology 30 (10), 863–866.
D'Alessandro, A., La Perna, R., Ciaranfi, N., 2003. Response of macrobenthos to changes in paleoenvironment in the Lower-Middle Pleistocene (Lucania Basin, southern Italy). Il Quaternario 16, 167–182.
Darling, K.F., Kucera, M., Kroon, D., Wade, C.M., 2006. A resolution for the coiling direction paradox in Neogloboquadrina pachyderma. Paleoceanography 21 (2), PA2011.
De Rijk, S., Rohling, E.J., Hayes, A., 1999. Onset of climatic deterioration in the eastern Mediterranean around 7 ky BP; micropalaeontological data from Mediterranean sapropel interruptions. Mar. Geol. 153, 337–343.
Di Donato, V., Insinga, D.D., Iorio, M., Molisso, F., Rumolo, P., Cardines, C., Passaro, S., 2019. The palaeoclimatic and palaeoceanographic history of the Gulf of Taranto (Mediterranean Sea) in the last 15 ky. Glob. Planet. Change 172, 278–297. https://doi.org/10.1016/j.gloplacha.2018.10.014.
Di Stefano, E., Incarbona, A., 2004. High-resolution paleoenvironmental reconstruction of the ODP-963D Hole (Sicily Channel) during the last deglaciation, based on calcareous nannofossils. Mar. Micropaleontol. 52, 241–254.
Doglioni, C., Tropeano, M., Mongelli, F., Pieri, P., 1996. Middle-Late Pleistocene uplift of Puglia: an "anomaly" in the Apenninic foreland. Mem. Soc. Geol. Ital. 51, 101–117.
Edelman-Furstenberg, Y., Almogi-Labin, A., Hemleben, C., 2009. Palaeoceanographic evolution of the central Red Sea during the late Holocene. The Holocene 19, 117–127. https://doi.org/10.1177/0959683608098955.
Elderfield, H., Ferretti, P., Greaves, M., Crowhurst, S., McCave, I.N., Hodell, D., Piotrowski, A.M., 2012. Evolution of ocean temperature and ice volume through the mid-Pleistocene climate transition. Science 337, 704–709.
Emanuele, D., Ferretti, P., Palumbo, E., Amore, F.O., 2015. Sea-surface dynamics and palaeoenvironmental changes in the North Atlantic Ocean (IODP Site U1313) during Marine Isotope Stage 19 inferred from coccolithophore assemblages. Palaeogeogr. Palaeoclimatol. Palaeoecol. 430, 104–117.
Emeis, K., Sakamoto, T., Wehausen, R., Brumsack, H.J., 2000a. The sapropel record of the eastern Mediterranean Sea - results of Ocean Drilling Program Leg 160. Palaeogeogr. Palaeoclimatol. Palaeoecol. 158, 371–395.
Emeis, K.-C., Struck, U., Schulz, H.-M., Bernasconi, S., Sakamoto, T., Martinez-Ruiz, F., 2000b. Temperature and salinity of Mediterranean Sea surface waters over the last 16 000 years: constraints on the physical environment of S1 sapropel formation based on stable oxygen isotopes and alkenone unsaturation ratios. Palaeogeogr. Palaeoclimatol. Palaeoecol. 158, 259–280.
Fairbanks, R.G., Sverdlove, M., Free, R., Wiebe, P.H., Bé, A.W.H., 1982. Vertical distribution of living planktonic foraminifera from the Panama Basin. Nature 298, 841–844.
Ferretti, P., Crowhurst, S.J., Naafs, B.D.A., Barbante, C., 2015. The Marine Isotope Stage 19 in the mid-latitude North Atlantic Ocean: astronomical signature and intra-interglacial variability. Quat. Sci. Rev. 108, 95–110.
Fletcher, C.G., Kushner, P.J., Hall, A., Quet, X., 2009. Circulation responses to snow albedo feedback in climate change. Geophys. Res. Lett. 36, L09702. https://doi.org/10.1029/2009GL038011.
Flores, J.A., Sierro, F.J., 1997. Revised technique for calculation of calcareous nannofossil accumulation rates. Micropaleontology 43, 321–324.
Fraile, I., Schulz, M., Mulitza, S., Kucera, M., 2008. Predicting the global distribution of planktonic foraminifera using a dynamic ecosystem model. Biogeosciences 5, 891–911.
Frigola, J., Moreno, A., Cacho, I., Canals, M., Sierro, F.J., Flores, J.A., Grimalt, J.O., 2008. Evidence of abrupt changes in Western Mediterranean Deep Water circulation during the last 50 kyr: A high-resolution marine record from the Balearic Sea. Quat. Int. 181, 88–104. https://doi.org/10.1016/j.quaint.2007.1006.1016.
Gačić, M., Eusebi Borzelli, G.L., Civitarese, G., Cardin, V., Yari, S., 2010. Can internal processes sustain reversals of the ocean upper circulation? The Ionian Sea example.

Gephys. Res. Lett. 37, L09608. https://doi.org/10.1029/2010GL043216.
Ganopolski, A., Rahmstorf, S., 2001. Rapid changes of glacial climate simulated in a coupled model. Nature 409, 153–158.
Geisen, M., Billard, C., Broerse, A.T.C., Cros, L., Probert, I., Young, J.R., 2002. Life-cycle associations involving pairs of holococcolithophorid species: intraspecific variation or cryptic speciation? Eur. J. Phycol. 37, 531–550.
Geraga, M., Tsaila-Monopolis, S., Ioakim, C., Papatheodorou, G., Ferentinos, G., 2000. Evaluation of palaeoenvironmental changes during the last 18,000 years in the Myrtoon basin, SW Aegean Sea. Palaeogeogr. Paleoclimatol. Palaeoecol. 156, 1–17.
Geraga, M., Tsaila-Monopolis, S., Ioakim, C., Papatheodorou, G., Ferentinos, G., 2005. Shortterm climate changes in the southern Aegean Sea over the last 48,000 years. Palaeogeogr. Palaeoclimat. Palaeoecol. 220, 311–332.
Geraga, M., Mylona, G., Tsaila-Monopolis, S., Papatheodorou, G., Ferentinos, G., 2008. Northeastern Ionian Sea: palaeoceanographic variability over the last 22 ka. J. Mar. Syst. 74, 623–638.
Geraga, M., Ioakim, Chr, Lykousis, V., Tsaila-Monopolis, St, Mylona, G., 2010. The high-resolution palaeoclimatic and palaeoceanographic history of the last 24,000 years in the central Aegean Sea, Greece. Palaeogeogr. Palaeoclimatol. Palaeoecol. 287, 101–115.
Giaccio, B., Regattieri, E., Zanchetta, G., Nomade, S., Renne, P.R., Sprain, C.J., Drysdale, R.N., Tzedakis, P.C., Messina, P., Scardia, G., Sposato, A., Bassinot, F., 2015. Duration and dynamics of the best orbital analogue to the present interglacial. Geology. https://doi.org/10.1130/G36677.1.
Girone, A., 2005. Response of otolith assemblages to sea-level fluctuations at the Lower Pleistocene Montalbano Jonico section (southern Italy). Bollettino della Società Paleontologica Italiana 44 (1), 35–45.
Girone, A., Capotondi, L., Ciaranfi, N., Di Leo, P., Lirer, F., Maiorano, P., Marino, M., Pelosi, N., Pulice, I., 2013. Paleoenvironmental change at the lower Pleistocene Montalbano Jonico section (southern Italy): global versus regional signals. Palaeogeogr. Palaeoclimatol. Palaeoecol. 371, 62–79.
Giunta, S., Negri, A., Maffioli, P., Sangiorgi, F., Capotondi, L., Morigi, C., Principato, M.S., Corselli, C., 2006. Phytoplankton dynamics in the eastern Mediterranean Sea during marine isotopic stage 5e. Palaeogeogr. Palaeoclimatol. Palaeoecol. 235, 28–47.
Goudeau, M.-L.S., Grauel, A.L., Bernasconi, S.M., de Lange, G.J., 2013. Provenance of surface sediments along the southeastern Adriatic coast off Italy: an overview. Estuar. Coast. Shelf Sci. 134, 45–56.
Grauel, A.L., Bernasconi, S.M., 2010. Core-top calibration of $\delta^{18}O$ and $\delta^{13}C$ of G. ruber (white) and U. mediterranea along the southern Adriatic coast of Italy. Mar. Micropaleontol. 77 (3–4), 175–186 (12).
Hayes, A., Rohling, E.J., De Rijk, S., Kroon, D., Zachariasse, W.J., 1999. Mediterranean planktonic foraminiferal faunas during the last glacial cycle. Mar. Geol. 153, 239–252.
Hayes, A., Kucera, M., Kallel, N., Sbaffi, L., Rohling, E.J., 2005. Glacial Mediterranean sea surface temperatures reconstructed from planktonic foraminiferal assemblages. Quat. Sci. Rev. 24, 999–1016.
Head, M., 2019. Formal subdivision of the Quaternary System/Period: Present status and future directions. Quat. Int. https://doi.org/10.1016/j.quaint.2019.05.018.
Hemleben, C., Spindler, M., Anderson, O.R., 1989. Modern Planktonic Foraminifera. Springer-Verlag, New York (363 pp).
Hodell, D., Lourens, L., Crowhurst, S., Konijnendijk, T., Tjallingii, R., Jimenez- Espejo, F., Skinner, L., Tzedakis, P.C., Shackleton Site Project Members, 2015. A reference time scale for site U1385 (Shackleton site) on the SW Iberian margin. Glob. Planet. Change 133, 48–64.
Hurrell, J.W., Hoerling, M.P., Phillips, A., Xu, T., 2004. Twentieth century north Atlantic climate change. Part I: assessing determinism. Clim. Dyn. 23, 371–389.
Incarbona, A., Sprovieri, M., Di Stefano, A., Di Stefano, E., Salvagio Manta, D., Pelosi, N., Ribera d'Alcalà, M., Sprovieri, R., Ziveri, P., 2013. Productivity modes in the Mediterranean Sea during Dansgaard-Oeschger (20,000-70,000 yr ago) oscillations. Palaeogeogr. Palaeoclimatol. Palaeoecol. 392, 128–137.
Johannessen, T., Jansen, E., Flatoy, A., Ravelo, A.C., 1994. The relationship between surface watermasses, oceanographic fronts and paleoclimatic proxies in surface sediments of the Greenland, Iceland and Norwegian seas. In: Zahn, R., Pedersen, T.F., Kaminski, M.A., Labeyrie, L. (Eds.), Carbon Cycling in the Glacial Ocean: Constraints on the Ocean's Role in Global Change. NATO Asi Series, I, 17. Springer, Heidelberg, pp. 61–86.
Kleiven, H., Hall, I.R., McCave, I.N., Knorr, G., Jansen, E., 2011. North Atlantic coupled deep-water flow and climate variability in the middle Pleistocene. Geology 39 (4), 343–346.
Konijnendijk, T.Y.M., Ziegler, M., Lourens, L.J., 2014. Chronological constraints on Pleistocene sapropel depositions from high-resolution geochemical records of ODP Sites 967 and 968. Newsl. Stratigr. 47 (3), 263–282.
Kontiokis, G., 2016. Late Quaternary paleoenvironmental reconstruction and paleoclimatic implications of the Aegean Sea (eastern Mediterranean) based on paleoceanographic indexes and stable isotopes. Quat. Int. 401, 28–42.
Kwiecien, O., Arz, H.W., Lamy, F., Plessen, B., Bahr, A., Haug, G.H., 2009. North Atlantic control on precipitation pattern in the eastern Mediterranean/Black Sea region during the last glacial. Quat. Res. 71, 375–384.
Laskar, J., Robutel, P., Joutel, F., Gastineau, M., Correia, A.C.M., Levrard, B., 2004. A long term numerical solution for the insolation quantities of the Earth. Astron. Astrophys. 428, 261–285. https://doi.org/10.1051/0004-6361:20041335.
Leaman, K.D., Schott, F.A., 1991. Hydrographyc structure of the convection regime in the Gulf of Lions: winter 1987. J. Phys. Oceanogr. 21, 575–598.
Lirer, F., Sprovieri, M., Ferraro, L., Vallefuoco, M., Capotondi, L., Cascella, A., Petrosino, P., Insinga, D.D., Pelosi, N., Tamburrino, S., Lubritto, C., 2013. Integrated stratigraphy for the late Quaternary in the eastern Tyrrhenian sea. Quat. Int. 292, 71–85.
Locarnini, R.A., Mishonov, A.V., Antonov, J.I., Boyer, T.P., Garcia, H.E., 2010. World Ocean Atlas 2009. Volume 1: Temperature; NOAA Atlas NESDIS 68. NOAA, U.S. Government Printing Office, Washington D.C.
Lourens, L.J., 2004. Revised tuning of Ocean Drilling Program Site 964 and KC01B (Mediterranean) and implications for the δ18O, tephra, calcareous nannofossil, and geomagnetic reversal chronologies of the past 1.1 Myr. Paleoceanography 19, PA3010.
Lourens, L., Hilgen, F., Shackleton, N.J., Laskar, J., Wilson, D., 2004. The Neogene period. In: Gradstein, F.M., Ogg, J.G., Smith, A.G. (Eds.), A Geological Time Scale. Cambridge University Press, pp. 409–440.
Maheras, P., Xoplaki, E., Kutiel, H., 1999. Wet and dry monthly anomalies across the Mediterranean basin and their relationship with circulation 1860–1990. Theor. Appl. Climatol. 64, 189–199.
Maiorano, P., Aiello, G., Barra, D., Di Leo, P., Joannin, S., Lirer, F., Marino, M., Pappalardo, A., Capotondi, L., Ciaranfi, N., Stefanelli, S., 2008. Paleoenvironmental changes during sapropel 19 (i-cycle 90) deposition: evidences from geochemical, mineralogical and microplaoentological proxies in the mid Pleistocene Montalbano Jonico land section (southern Italy). Palaeogeogr. Palaeoclimatol. Palaeoecol. 257, 308–334.
Maiorano, P., Capotondi, L., Ciaranfi, N., Girone, A., Lirer, F., Marino, M., Pelosi, N., Petrosino, P., Piscitelli, A., 2010. Vrica-Crotone and Montalbano Jonico sections: a potential unit-stratotype of the Calabrian Stage. Episodes 33, 218–233.
Maiorano, P., Tarantino, F., Marino, M., De Lange, G.J., 2013. Paleoenvironmental conditions at Core KC01B (Ionian Sea) through MIS 13-9: evidence from calcareous nannofossil assemblages. Quat. Int. 288, 97–111.
Maiorano, P., Marino, M., Balestra, B., Flores, J.A., Hodell, D.A., Rodrigues, T., 2015. Coccolithophore variability from the Shackleton Site (IODP Site U1385) through MIS 16-10. Glob. Planet. Change 133, 35–48.
Maiorano, P., Bertini, A., Capolongo, D., Eramo, G., Gallicchio, S., Girone, A., Pinto, D., Toti, F., Ventruti, G., Marino, M., 2016a. Climate signatures through the Marine Isotope Stage 19 in the Montalbano Jonico section (Southern Italy): a land-sea perspective. Palaeogeogr. Palaeoclimatol. Palaeoecol. 461, 341–361.
Maiorano, P., Girone, A., Marino, M., Kucera, M., Pelosi, N., 2016b. Sea surface water variability during the Mid-Brunhes inferred from calcareous plankton in the western Mediterranean (ODP Site 975). Palaeogeogr. Palaeoclimatol. Palaeoecol. 459, 229–248.
Malanotte-Rizzoli, P., Manca, B.B., Ribera d'Alcala, M., Theocharis, A., Brenner, S., Budillon, G., Ozsoy, E., 1999. The eastern Mediterranean in the 80s and in the 90s: The big transition in the intermediate and deep circulations. Dyn. Atmos. Oceans 29, 365–395.
Malanotte-Rizzoli, P., Artale, V., Borzelli-Eusebi, G.L., Brenner, S., Crise, A., Gačić, M., Kress, N., Marullo, S., Ribera d'Alcalà, M., Sofianos, S., Tanhua, T., Theocharis, A., Alvarez, M., Ashkenazy, Y., Bergamasco, A., Cardin, V., Carniel, S., Civitarese, G., D'Ortenzio, F., Font, J., Garcia-Ladona, E., Garcia-Lafuente, J.M., Gogou, A., Gregoire, M., Hainbucher, D., Kontoyannis, H., Kovacevic, V., Kraskapoulou, E., Kroskos, G., Incarbona, A., Mazzocchi, M.G., Orlic, M., Ozsoy, E., Pascual, A., Poulain, P.M., Roethe, W., Rubino, A., Schroeder, K., Siokou-Frangou, J., Souvermezoglou, E., Sprovieri, M., Tintoré, J., Triantafyllou, G., 2014. Physical forcing and physical/biochemical variability of the Mediterranean Sea: a review of unresolved issues and directions for future research. Ocean Sci. 10, 281–322.
Mallo, M., Ziveri, P., Mortyn, P.G., Schiebel, R., Grelaud, M., 2017. Low planktic foraminiferal diversity and abundance observed in a spring 2013 west-east Mediterranean Sea plankton tow transect. Biogeosciences 14, 2245–2266.
Marino, M., Maiorano, P., Flower, B.P., 2011. Calcareous nannofossil changes during the Mid- Pleistocene revolution: paleoecologic and paleoceanographic evidence from North Atlantic Site 980/981. Palaeogeogr. Palaeoclimatol. Palaeoecol. 306 (1–2), 58–69.
Marino, M., Maiorano, P., Tarantino, F., Voelker, A., Capotondi, L., Girone, A., Lirer, F., Flores, J.-A., Naafs, B.D.A., 2014. Coccolithophores as proxy of seawater changes at orbital- to-millennial scale during middle Pleistocene Marine Isotope Stages 14–9 in North Atlantic core MD01-2446. Paleoceanography 29. https://doi.org/10.1002/2013PA002574.
Marino, M., Bertini, A., Ciaranfi, N., Aiello, G., Barra, D., Gallicchio, S., Girone, A., La Perna, R., Lirer, F., Maiorano, P., Petrosino, P., Toti, F., 2015. Paleoenvironmental and climatostratigraphic insights for Marine Isotope Stage 19 (Pleistocene) at the Montalbano Jonico section, South Italy. Quat. Int. 383, 104–115. https://doi.org/10.1016/j.quaint.2015.01.043.
Marino, M., Aiello, G., Barra, D., Bertini, A., Gallicchio, S., Girone, A., La Perna, R., Lirer, F., Maiorano, P., Petrosino, P., Quivelli, O., Toti, F., Ciaranfi, N., 2016. The Montalbano Jonico section (South Italy) as a reference for the Early/Middle Pleistocene boundary. Alp. Mediterr. Quat. 29 (1), 45–57.
Marino, M., Girone, A., Maiorano, P., Di Renzo, R., Piscitelli, A., Flores, J.-A., 2018. Calcareous plankton and the mid-Brunhes climate variability in the Alboran Sea (ODP Site 977). Palaeogeogr. Palaeoclimatol. Palaeoecol. 508, 91–106.
Mariolopoulos, E.G., 1961. An outline of the climate of Greece. vol. 6 Publications of the Meteorological Institute of the University of Athens (51 pp).
Martinez, J.I., Mora, G., Barrows, T.T., 2007. Paleoceanographic conditions in the western Caribbean Sea for the last 560 kyr as inferred from planktonic foraminifera. Mar. Micropaleontol. 64, 177–188.
Martin-Garcia, G.M., Alonso-Garcia, M., Sierro, F.J., Hodell, D.A., Flores, J.A., 2015. Severe cooling episodes at the onset of deglaciations on the Southwestern Iberian margin from MIS 21 to 13 (IODP site U1385). Glob. Planet. Change 135, 159–169.
Martrat, B., Jimenez-Amat, P., Zahn, R., Grimalt, J.O., 2014. Similarities and dissimilarities between the last two deglaciations and interglaciations in the North Atlantic region. Quat. Sci. Rev. 99, 112–134.
Maselli, V., Hutton, E.W., Kettner, A.J., Syvtski, J.P.M., Trincardi, F., 2011. High-frequency sea level and sediment supply fluctuations during Termination I: An

integrated sequence-stratigraphy and modeling approach from the Adriatic Sea (Central Mediterranean). Mar. Geol. 287 (54-70 pp).
McIntyre, A., Bé, A.H.W., 1967. Modern coccolithophores of the Atlantic Ocean - I. Placolith and cyrtoliths. Deep Sea Res 14, 561–597.
Miller, K.G., Wright, J.D., 2017. Success and failure in Cenozoic global correlations using golden spikes: A geochemical and magnetostratigraphic perspective. Episodes 40 (1), 1–22.
Milligan, T.G., Cattaneo, A., 2007. Sediment Dynamics in the Western Adriatic Sea: From transport to stratigraphy. Cont. Shelf Res. 27, 287–295.
Molfino, B., McIntyre, A., 1990. Nutricline variation in the equatorial Atlantic coincident with the Younger Dryas. Paleoceanography 5, 997–1008.
Morard, R., Quillévéré, F., Escarguel, G., Ujiie, Y., de Garidel-Thoron, T., Norris, R.D., de Vargas, C., 2009. Morphological recognition of cryptic species in the planktonic foraminifer Orbulina universa. Mar. Micropaleontol. 71, 148–165.
Moreno, A., Cacho, I., Canals, M., Prins, M.A., Sánchez-Goñi, M.F., Grimalt, J.O., Weltje, G.J., 2002. Saharan dust transport and high-latitude glacial climatic variability: the Alboran Sea record. Quat. Res. 58 (3), 318–328.
Moreno, A., Cacho, I., Canals, M., Grimalt, J.O., Sanchez-Vidal, A., 2004. Millennial-scale variability in the productivity signal from the Alboran Sea record, Western Mediterranean Sea. Palaeogeogr. Palaeoclimatol. Palaeoecol. 211 (3–4), 205–219.
Moreno, A., Cacho, I., Canals, M., Grimalt, J.O., Sánchez-Goñi, M.F., Shackleton, N., Sierro, F.J., 2005. Links between marine and atmospheric processes oscillating on a millennial time-scale. A multi-proxy study of the last 50,000 yr from the Alboran Sea (Western Mediterranean Sea). Quat. Sci. Rev. 24 (14–15), 1623–1636.
Moscariello, A., Ravazzi, C., Brauer, A., Mangili, C., Chiesa, S., Rossi, S., de Beaulieu, J.L., Reille, M., 2000. A long lacustrine record from the Pianico-Sellere basin (Middle-Late Pleistocene, Nothern Italy). Quat. Int. 73-74, 47–68.
Müller, P.J., Kirst, G., Ruhland, G., von Storch, I., Rosel-Melé, A., 1998. Calibration of the alkenone paleotemperature index $U_{37}^{K'}$ based on core-tops from the eastern Aouth Atlantic and the global ocean (60N-60S). Geochim. Cosmochim. Acta 62, 1757–1772.
Narciso, A., Flores, J.-A., Cachão, M., Sierro, F.-J., Colmenero-Hidalgo, E., Piva, A., Asioli, A., 2010. Sea surface dynamics and coccolithophore behaviour during sapropel deposition of Marine Isotope Stage 7, 6 and 5 in the Western Adriatic Sea. Rev. Esp. Micropaleontol. 42, 345–358.
Naughton, F., Drago, T., Sánchez Goñi, M.F., Freitas, M.C., 2011. Climate variability in the North-Western Iberian Peninsula during the last deglaciation. In: Oceans and the Atmospheric Carbon Content. Springer, Netherlands, pp. 1–22.
Naughton, F., Sánchez Goñi, M.F., Rodrigues, T., Salgueiro, E., Costas, S., Desprat, S., Duprat, J., Michel, E., Rossignol, L., Zaragosi, S., Voelker, A.H.L., Abrantes, F., 2016. Climate variability across the last deglaciation in NW Iberia and its margin. Quat. Int. 414, 9–22.
Nomade, S., Bassinot, F., Marino, M., Simon, Q., Dewilde, F., Maiorano, P., Esguder, G., Blamart, D., Girone, A., Scao, V., Pereira, A., Toti, F., Bertini, A., Combourieu-Nebout, N., Peral, M., Bourles, D., Petrosino, P., Gallicchio, S., Ciaranfi, N., 2019. High-resolution foraminifer stable isotope record of MIS 19 at Montalbano Jonico, southern Italy: a window into Mediterranean climatic variability during a low-eccentricity interglacial. Quat. Sci. Rev. 205, 106–125.
North Greenland Ice Core Project members, 2004. High-resolution record of Northern Hemisphere climate extending into the last interglacial period. Nature 431, 147–151.
Palumbo, E., Flores, J.A., Perugia, C., Petrillo, Z., Voelker, A.H.L., Amore, F.O., 2013. Millennial-scale coccolithophore paleoproductivity and surface water changes between 445 and 360 ka (Marine Isotope Stages 12/11) in the Northeast Atlantic. Palaeogeogr. Palaeoclimatol. Palaeoecol. 383-384, 27–41.
Parente, A., Cachão, M., Baumann, K.-H., de Abreu, L., Ferreira, J., 2004. Morphometry of Coccolithus pelagicus s.l. (Coccolithophore, Haptophyta) from offshore Portugal, during the last 200 kyr. Micropaleontology 50, 107–120.
Patacca, E., Scandone, P., 2007. Geology of the Southern Apennines. Bollettino della Società Geologica Italiana, Special Issue 7, 75–119.
Paterne, M., Nejib, K., Labeyrie, L.D., Vautravers, M. Duplessy J.C., Rossignol-Strick, M., Cortijo, E., Arnold, M., Fontugne, M. R., 1999. Hydrological relationship between the North Atlantic Ocean and the Mediterranean Sea during the past 15-75 kyr. Paleoceanography 14 (5), 626–638.
Peral, M., Blamart, D., Bassinot, F., Daëron, M., Dewilde, F., Rebaubier, H., Nomade, S., Girone, A., Marino, M., Maiorano, P., Ciaranfi, N., 2020. Changes in temperature and oxygen isotopic composition of Mediterranean water during the Mid-Pleistocene transition in the Montalbano Jonico section (southern Italy) using the clumped-isotope thermometer. Palaeogeogr. Palaeoclimatol. Palaeoecol. 544, 109603. https://doi.org/10.1016/j.palaeo.2020.109603.
Pérez-Folgado, M., Sierro, F.J., Flores, J.A., Cacho, I., Grimalt, J.O., Zahn, R., Shackleton, N., 2003. Western Mediterranean planktonic foraminifera events and millennial climatic variability during the last 70 kyr. Mar. Micropaleontol. 48, 49–70.
Pescatore, T., Pieri, P., Sabato, L., Senatore, M.R., Gallicchio, S., Boscaino, M., Cilumbriello, A., Quarantiello, R., Capretto, G., 2009. Stratigrafia dei depositi pleistocenico-olocenici dell'area costiera di Metaponto compresa fra Marina di Ginosa ed il Torrente Cavone (Italia meridionale): Carta Geologica in scala 1:25.000. Il Quaternario 22 (2), 307–323.
Petrosino, P., Jicha, B.R., Mazzeo, F.C., Ciaranfi, N., Girone, A., Maiorano, P., Marino, M., 2015. The Montalbano Jonico marine succession: An archive for distal tephra layers at the Early-Middle Pleistocene boundary in southern Italy. Quat. Int. 383, 89–103. https://doi.org/10.1016/j.quaint.2014.10.049.
Pinardi, N., Masetti, E., 2000. Variability of the large scale general circulation of the mediterranean sea from observations and modelling: a review. Palaeogeogr. Palaeoclimatol. Palaeoecol. 158 (2000), 153173.
Piva, A., Asioli, A., Trincardi, F., Schneider, R.R., Vigliotti, L., 2008. Late-Holocene climate variability in the Adriatic Sea (Central Mediterranean). The Holocene 18 (1), 153–167.
Pol, K., Masson-Delmotte, V., Johnsen, S., Bigler, M., Cattani, O., Durand, G., Falourd, S., Jouzel, J., Minster, B., Parrenin, F., Ritz, C., Steen-Larsen, H.C., Stenni, B., 2010. New MIS 19 EPICA Dome C high-resolution deuterium data: hints for a problematic preservation of climate variability in the "oldest ice". Earth Planet. Sci. Lett. 298 (1–2), 95–103. https://doi.org/10.1016/j.epsl.2010.07.030. (2010).
Poulain, P.-M., 2001. Adriatic Sea surface circulation as derived from drifter data between 1990 and 1999. J. Mar. Syst. 29, 3–32.
Poulos, S.E., Drakopoulos, P.G., Collins, M.B., 1997. Seasonal variability in sea surface oceanographic conditions in the Aegean Sea (Eastern Mediterranean): an overview. J. Mar. Syst. 13, 225–244.
Pros, J., Kotthoff, U., Müller, U.C., Peyron, O., Dormoy, I., Schmiedl, G., Kalaitzidis, S., Smith, A.M., 2009. Massive perturbation in terrestrial ecosystems of the Eastern Mediterranean region associated with the 8.2 kyr B.P. climatic event. Geology 37 (10), 887–890. https://doi.org/10.1130/G25739A.1.
Pujol, C., Vergnaud-Grazzini, C., 1995. Distribution patterns of live planktic foraminifers as related to regional hydrography and productive systems of the Mediterranean Sea. Mar. Micropaleontol. 25, 187–217.
Quivelli, O., 2020. Coccolithophores and biomarkers as paleoclimatic and paleoceanographic indicators during Marine Isotope Stage 20–18. PhD Thesis, 189 pp. Università degli Studi di Bari Aldo Moro, Bari, Italy.
Quivelli, O., Marino, M., Rodrigues, T., Girone, A., Maiorano, P., Abrantes, F., Salgueiro, E., Bassinot, F., 2020. Surface and deep water variability in the Western Mediterranean (ODP Site 975) during insolation cycle 74: High-resolution calcareous plankton and molecular biomarker signals. Palaeogeogr. Palaeoclimatol. Palaeoecol. 542, 109583. https://doi.org/10.1016/j.palaeo.2019.109583.
Railsback, L.C., Gibbard, P.L., Heas, M.J., Voarintsoa, N.R.G., Tucanne, S., 2015. An optimized scheme of lettered marine isotope substages for the last 1.0 million years, and the climatostratigraphic nature of isotope stages and substages. Quat. Sci. Rev. 111, 94–106.
Raymo, M.E., Ruddiman, W.F., Rind, D., 1990. Climatic effects of reduced Arctic sea ice limits in the GISS-II GCM. Paleoceanography 5, 367–382.
Raymo, M.E., Oppo, D.W., Curry, W., 1997. The mid-Pleistocene climate transition: a deep-sea carbon isotopic perspective. Paleoceanography 12, 546–559.
Regattieri, E., Giaccio, B., Mannella, G., Zanchetta, G., Nomade, S., Tognarelli, A., Perchiazzi, N., Vogel, H., Boschi, C., Neil, R.D., Wagner, B., Gemelli, M., Tzedakis, P., 2019. Frequency and dynamics of millennial-scale variability during Marine Isotope Stage 19: Insights from the Sulmona Basin (central Italy). Quat. Sci. Rev. 214, 28–43.
Repschläger, J., Weinelt, M., Kinkel, H., Andersen, N., Garbe Schönberg, D., Schwab, C., 2015. Response of the subtropical North Atlantic surface hydrography on deglacial and Holocene AMOC changes. Paleoceanography 30, 456–476. https://doi.org/10.1002/2014pa002637.
Reynolds, L.A., Thunell, R.C., 1986. Seasonal production and morphologic variation of Neogloboquadrina pachyderma (Ehrenberg) in the northeast Pacific. Micropaleontology 32, 1–18.
Rio, D., Raffi, I., Villa, G., 1990. Pliocene-Pleistocene distribution patterns in the Western Mediterranean. In: Karstetn, K.A., Mascle, J. (Eds.), Proceedings of ODP, Scientific Results. vol. 107. pp. 513–533.
Roberts, N., Jones, M.D., Benkaddur, A., Eastwood, W.J., Filippi, M.L., Frogley, M.R., Lamb, H.F., Leng, M.J., Reed, J.M., Stein, M., Stevens, L., Valero-Garces, B., Zanchetta, G., 2008. Stable isotope records of Late Quaternary climate and hydrology from Mediterranean lakes: the ISOMED synthesis. Quat. Sci. Rev. 27, 2426–2441.
Rodrigo-Gámiz, M., Martínez-Ruiz, F., Jiménez-Espejo, F.J., Gallego-Torres, D., Nieto-Moreno, V., Romero, O., Ariztegui, D., 2011. Impact of climate variability in the western Mediterranean during the last 20,000 years: oceanic and atmospheric responses. Quat. Sci. Rev. 30 (15), 2018–2034.
Rodrigues, T., Voelker, A.H.L., Grimalt, J.O., Abrantes, F., Naughton, F., 2011. Iberian margin sea surface temperature during MIS 15 to 9 (580–300 ka): glacial suborbital variability versus interglacial stability. Paleoceanography 26, PA1204. https://doi.org/10.1029/2010PA001927.
Rodrigues, T., Alonso-García, M., Hodell, D.A., Rufino, M., Naughton, F., Grimalt, J.O., Voelker, A.H.L., Abrantes, F., 2017. A 1-Ma record of sea surface temperature and extreme cooling events in the North Atlantic: a perspective from the Iberian margin. Quat. Sci. Rev. 172, 118–130.
Rogerson, M., Cacho, I., Jimenez-Espejo, F., Reguera, M.I., Sierro, F.J., Martinez-Ruiz, F., Frigola, J., Canals, M., 2008. A dynamic explanation for the origin of the western Mediterranean organic rich layers. Geochem. Geophys. Geosyst. 9, Q07U01. https://doi.org/10.1029/2007GC001936.
Rohling, E.J., Gieskes, W.W.C., 1989. Late Quaternary changes in Mediterranean intermediate water density and formation rate. Paleoceanography 4, 531–545.
Rohling, E.J., Jorissen, F.J., Vergnaud Grazzini, C., Zachariasse, W.J., 1993. Northern Levantine and Adriatic Quaternary planktic foraminifera; reconstruction of paleoenvironmental gradients. Mar. Micropaleontol. 21, 191–218.
Rohling, E.J., den Dulk, M., Pujol, C., Vergnaud-Grazzini, C., 1995. Abrupt hydrographic changes in the Alboran Sea (western Mediterranean) around 8000 yrs BP. Deep-Sea Res. 42, 1609–1619.
Rohling, E.J., Jorissen, F.J., De Stigter, H.C., 1997. 200-year interruption of Holocene sapropel formation in the Adriatic Sea. J. Micropalaeontol. 16 (2), 97–108.
Rohling, E.J., Mayewski, P.A., Hayes, A., Abu-Zied, R.H., Casford, J.S.L., 2002. Holocene atmosphere-ocean interactions: records from Greenland and the Aegean Sea. Clim. Dyn. 18, 587–593.
Rohling, E.J., Hayes, A., Mayewski, P.A., Kucera, M., 2009. Holocene climate variability in the eastern Mediterranean, and the End of the Bronze Age. In: Bachhuber, C., Roberts, G. (Eds.), Forces of Transformation: The End of the Bronze Age in the Mediterranean. Oxbow Books, Oxford, UK, pp. 2–5.
Rossi, S., 2003. Etude pollinique de la séequence lacustre Pléistocène de Pianico-Sèllere (Italie). Ph.D. Thesis. Universitè de Droit d'Economie et des Sciences d'Aix Marseille

III.
Rouis-Zargouni, I., Turon, J.-L., Londeix, L., Essallami, L., Kallel, N., Sicre, M.-A., 2010. Environmental and climatic changes in the central Mediterranean Sea (Siculo–Tunisian Strait) during the last 30 ka based on dinoflagellate cyst and planktonic foraminifera assemblages. Palaeogeogr. Palaeoclimatol. Palaeoecol. 285, 17–29.
Ruddiman, W., Fuller, D., Kutzbach, J., Tzedakis, P., Kaplan, J., Ellis, E., Vavrus, S., Roberts, C., Fyfe, R., He, F., 2016. Late Holocene climate: Natural or anthropogenic? Rev. Geophys. 54 (1), 93–118.
Saaroni, H., Bitan, A., Alpert, P., Ziv, B., 1996. Continental polar outbreaks into the Levant and Eastern Mediterranean. Int. J. Climatol. 16, 1175–1191.
Saavedra-Pellitero, M., Flores, J.A., Baumann, K.-H., Sierro, F.J., 2010. Coccolith distribution patterns in surface sediments of equatorial and southeastern Pacific Ocean. Geobios 43, 131–149.
Sánchez Goñi, M.S., Cacho, I., Turon, J.L., Guiot, J., Sierro, F.J., Peypouquet, J.P., Shackleton, N.J., 2002. Synchroneity between marine and terrestrial responses to millennial scale climatic variability during the last glacial period in the Mediterranean region. Clim. Dyn. 19 (1), 95–105.
Sánchez Goñi, M.F., Rodrigues, T., Hodell, D.A., Polanco-Martínez, J.M., Alonso-García, M., Hernández-Almeida, I., Desprat, S., Ferretti, P., 2016. Tropically-driven climate shifts in southwestern Europe during MIS 19, a low eccentricity interglacial. Earth Planet. Sci. Lett. 448, 81–93.
Sangiorgi, F., Dinelli, E., Maffioli, P., Capotondi, L., Giunta, S., Morigi, C., Principato, M.S., Negri, A., Emeis, K.-C., Corselli, C., 2006. Geochemical and micro-paleontological characterization of a Mediterranean sapropel S5: a case study from core BAN89GC09 (south of Crete). Palaeogeogr. Palaeoclimatol. Palaeoecol. 235, 192–207.
Sauer, D., Wagner, S., Brückner, H., Scarciglia, F., Mastronuzzi, G., 2010. Soil development on marine terraces near Metaponto (Gulf of Taranto, Southern Italy). Quat. Int. 222, 48–63.
Savini, A., Corselli, C., 2010. High-resolution bathymetry and acoustic geophysical data from Santa Maria di Leuca Cold Water Coral province (Northern Ionian Sea-Apulian continental slope). Deep-Sea Res. II 57, 326–344.
Sbaffi, L., Wezel, F.C., Kallel, N., Paterne, M., Cacho, I., Ziveri, P., Shackleton, N., 2001. Response of the pelagic environment to palaeoclimatic changes in the central Mediterranean Sea during the Late Quaternary. Mar. Geol. 178, 39–62.
Siani, G., Paterne, M., Colin, C., 2010. Late glacial to Holocene planktic foraminifera bioevents and climatic record in the South Adriatic Sea. J. Quat. Sci. 25, 808–821.
Siani, G., Magny, M., Paterne, M., Debret, M., Fontugne, M., 2013. Paleohydrology reconstruction and Holocene climate variability in the South Adriatic Sea. Clim. Past 9, 499–515. https://doi.org/10.5194/cp-9-499-2013.
Sierro, F.J., Hodell, D.A., Curtis, J.H., Flores, J.A., Reguera, I., Colmenero-Hidalgo, E., Bárcena, M.A., Grimalt, J.O., Cacho, I., Frigola, J., Canals, M., 2005. Impact of iceberg melting on Mediterranean thermohaline circulation during Heinrich events. Paleoceanography 20 PA2019.
Simon, Q., Bourlès, L.D., Bassinot, F., Nomade, S., Marino, M., Ciaranfi, N., Girone, A., Maiorano, P., Thouveny, N., Choya, S., Dewil, F., Scao, V., Isguder, G., Blamart, D., ASTER Team, 2017. Authigenic 10Be/9Be ratio signature of the Matuyama-Brunhes boundary in the Montalbano Jonico marine succession. Earth Planet. Sci. Lett. 460, 255–267. https://doi.org/10.1016/j.epsl.2016.11.052.
Simstich, J., Sarnthein, M., Erlenkeuser, H., 2003. Paired $\delta^{18}O$ signals of Neogloboquadrina pachyderma (s) and Turborotalita quinqueloba showthermal stratification structure in Nordic Seas. Mar. Micropaleontol. 48, 107–125.
Socal, G., Boldrin, A., Bianchi, F., Civitarese, G., De Lazzari, A., Rabitti, S., Totti, C., Turchetto, M.M., 1999. Nutrient, particulate matter and phytoplankton variability in the photic layer of the Otranto strait. J. Mar. Syst. 20, 381–398.
Spero, H.J., Williams, D.F., 1990. Evidence for seasonal low-salinity surface waters in the Gulf of Mexico over the last 16,000 years. Paleoceanography 5, 963–975. https://doi.org/10.1029/PA005i006p00963.
Spezzaferri, S., Kucera, M., Pearson, P.N., Wade, B.S., Rappo, S., Poole, C.R., Morard, R., Stalder, C., 2015. Fossil and genetic evidence for the polyphyletic nature of the planktonic foraminifera “Globigerinoides”, and description of the new genus Trilobatus. PLoS One 10 (5), e0128108. https://doi.org/10.1371/journal.pone.0128108.
Sprovieri, R., Di Stefano, E., Incarbona, A., Gargano, M.E., 2003. A high-resolution of the last deglaciation in the Sicily Channel based on foraminiferal and calcareous nannofossil quantitative distribution. Palaeogeogr. Palaeoclimatol. Palaeoecol. 202, 119–142.
Sprovieri, M., Di Stefano, E., Incarbona, A., Manta, D.S., Pelosi, N., d’Alcalà, M.R., Sprovieri, R., 2012. Centennial-to millennial-scale climate oscillations in the Central-Eastern Mediterranean Sea between 20,000 and 70,000 years ago: evidence from a high-resolution geochemical and micropaleontological record. Quat. Sci. Rev. 46, 126–135.
Stefanelli, S., 2003. Benthic foraminiferal assemblages as tools for paleoenvironmental reconstruction of the early-middle Pleistocene Montalbano Jonico composite section. Bollettino della Società Paleontologica Italiana 42, 281–299.
Stefanelli, S., 2004. Cyclic stages in oxygenation based on foraminiferal microhabitats: early-middle Pleistocene, Lucania basin, southern Italy. J. Micropaleontol. 23, 81–95.
Stefanelli, S., Capotondi, L., Ciaranfi, N., 2005. Foraminiferal record and environmental changes during the deposition of early-middle Pleistocene sapropels in southern Italy. Palaeogeogr. Palaeoclimatol. Palaeoecol. 216, 27–52.
Stein, R., Hefter, J., Grützner, J., Voelker, A., Naafs, B.D.A., 2009. Variability of surface water characteristics and Heinrich-like events in the Pleistocene mid-latitude North Atlantic Ocean: Biomarker and XRD records from IODP Site U1313 (MIS 16-9). Paleoceanography 24, PA2203. https://doi.org/10.1029/2008PA001639.
Thunell, R.C., 1978. Distribution of recent planktonic foraminifera in surface sediments of the Mediterranean Sea. Mar. Micropaleontol. 3, 147–173.
Tolderlund, D.S., Bé, A.W.H., 1971. Seasonal distribution of planktonic foraminifera in the western North Atlantic. Micropaleontolology 17, 297–329.
Toti, F., Bertini, A., Girone, A., Marino, M., Maiorano, P., Bassinot, F., Combourieu-Nebout, N., Nomade, S., Buccianti, A., 2020. Marine and terrestrial climate variability in the western Mediterranean Sea during marine isotope stages 20 and 19. Quat. Sci. Rev. 243. https://doi.org/10.1016/j.quascirev.2020.106486.
Triantaphyllou, M.V., Ziveri, P., Gogou, A., Marino, G., Lykousis, V., Boulobassi, Emeis, K.-C., Kouli, K., Dimiza, M., Rosell-Melé, A., Papanikolaou, M., Katsouras, G., Nunez, N., 2009. Late Glacial–Holocene climate variability at the south-eastern margin of the Aegean Sea. Mar. Geol. 266, 182–197.
Trotta, S., Marino, M., Maiorano, P., Girone, A., 2019. Climate variability through MIS 20-MIS 19 in core KC01B, Ionian Basin (central Mediterranean Sea). Alp. Med. Quat. 32 (2), 1–15. https://doi.org/10.26382/AMQ.2019.10.
Turchetto, M., Boldrin, A., Langone, L., Miserocchi, S., Tesi, T., Foglini, F., 2007. Particle transport in the Bari canyon (southern Adriatic Sea). Mar. Geol. 246, 231–247.
Tzedakis, P.C., Channell, J.E.T., Hodell, D.A., Kleiven, H.F., Skinner, L.C., 2012. Determining the natural length of the current interglacial. Nat. Geosci. 5. https://doi.org/10.1038/NGEO1358.
Ulbrich, U., Lionello, P., Belusic, D., Jacobeit, J., Knippertz, P., Kuglitsch, F.G., Ziv, B., 2012. Climate of the Mediterranean: synoptic patterns, temperature, precipitation, winds, and their extremes. In: The Climate of the Mediterranean Region-From the Past to the Future. Elsevier, pp. 301–346. https://doi.org/10.1016/B978-0-12-416042-2.00005-7.
Vetter, L., Spero, H.J., Eggins, S.M., Williams, C., Flower, B.P., 2017. Oxygen isotope geochemistry of Laurentide ice-sheet meltwater across Termination I. Quat. Sci. Rev. 178, 102–117.
Vezzani, L., 1967. I depositi plio-pleistocenici del litorale ionico della Lucania. In: Atti Acc. Gioenia Sc. Nat. in Catania, s. VI. vol. 18. pp. 159–180.
Vincent, E., Berger, W.H., 1981. Planktonic foraminifera and their use in Paleoceanography. In: Emiliani, C. (Ed.), The Oceanic Lithosphere The sea. vol. 7. John Wiley & Sons, New York, pp. 1025–1119.
Voelker, A.H.L., Rodrigues, T., Billups, K., Oppo, D., McManus, J., Stein, R., Hefter, J., Grimalt, J.O., 2010. Variations in mid-latitude North Atlantic surface water properties during the mid-Brunhes (MIS 9-14) and their implications for the thermohaline circulation. Clim. Past 6, 531–552.
von Grafenstein, R., Zamn, R., Tiedemann, R., Murat, A., 1999. Planktonic $\delta^{18}O$ records at Sites 976 and 977, Alboran Sea: stratigraphy, forcing and paleoceanographic implications. In: Zahn, R., Comas, M.C., Klaus, A. (Eds.), Proceedings of the Ocean Drilling Program, Scientific Results. vol. 161. pp. 469–479.
Wagner, B., Vogel, H., Francke, A., et al., 2019. Mediterranean winter rainfall in phase with African monsoons during the past 1.36 million years. Nature 573, 256–260. https://doi.org/10.1038/s41586-019-1529-0.
Weaver, P.P.E., Pujol, C., 1988. History of the last deglaciation in the Alboran Sea (western Mediterranean) and adjacent North Atlantic as revealed by coccolith floras. Paleogeogr. Paleoclimatol. Paleoecol. 64, 35–42.
Winter, A., Jordan, R.W., Roth, P.H., 1994. Biogeography of living coccolithophores in ocean waters. In: Siesser, W.G. (Ed.), Coccolithophores. Cambridge University Press, London, pp. 161–178.
Wright, A.K., Flower, B.P., 2002. Surface and deep ocean circulation in subpolar North Atlantic during the mid-Pleistocene revolution. Paleoceanography 17, 1068. https://doi.org/10.1029/2002PA000782.
Xoplaki, E., Gonzalez-Rouco, J.F., Luterbacher, J., Wanner, H., 2003. Mediterranean summer air temperature variability and its connection to the large-scale atmospheric circulation and SSTs. Clim. Dyn. 20 (7–8), 723–739.
Ziveri, P., Baumann, K.-H., Boeckel, B., Bollmann, Young, J., Young, Y.R., 2004. Biogeography of selected Holocene coccoliths in the Atlantic Ocean. In: Thierstein, H.R. (Ed.), Coccolithophores: From Molecular Processes to Global Impact. Springer, Berlin, pp. 403–428.
Zonneveld, K.A.F., Versteegh, G.J.M., Kodrans-Nsiah, M., 2008. Preservation and organic chemistry of Late Cenozoic organic-walled dinoflagellate cysts: a review. Mar. Micropaleontol. 86, 179–197.